

See discussions, stats, and author profiles for this publication at: <https://www.researchgate.net/publication/367558695>

Integrated network pharmacology and in-silico approaches to decipher the pharmacological mechanism of *Selaginella tamariscina* in the treatment of non-small cell lung cancer

Article in *Phytomedicine Plus* · January 2023

DOI: 10.1016/j.phyplu.2023.100419

CITATIONS

17

READS

176

7 authors, including:



Sunil Kumar

Shoolini University

12 PUBLICATIONS 144 CITATIONS

[SEE PROFILE](#)



Faheem Abbas

Tsinghua University Beijing China

62 PUBLICATIONS 429 CITATIONS

[SEE PROFILE](#)



Iqra Ali

COMSATS University Islamabad

11 PUBLICATIONS 41 CITATIONS

[SEE PROFILE](#)



Manoj K. Gupta

Central University of Haryana

81 PUBLICATIONS 1,173 CITATIONS

[SEE PROFILE](#)

Journal Pre-proof

Integrated network pharmacology and in-silico approaches to decipher the pharmacological mechanism of *Selaginella tamariscina* in the treatment of non-small cell lung cancer

Sunil Kumar , Faheem Abbas , Iqra Ali , Manoj K. Gupta , Saroj Kumar , Manoj Garg , Deepak Kumar

PII: S2667-0313(23)00015-5
DOI: <https://doi.org/10.1016/j.phyplu.2023.100419>
Reference: PHYPLU 100419



To appear in: *Phytomedicine Plus*

Received date: 15 November 2022
Revised date: 23 December 2022
Accepted date: 24 January 2023

Please cite this article as: Sunil Kumar , Faheem Abbas , Iqra Ali , Manoj K. Gupta , Saroj Kumar , Manoj Garg , Deepak Kumar , Integrated network pharmacology and in-silico approaches to decipher the pharmacological mechanism of *Selaginella tamariscina* in the treatment of non-small cell lung cancer, *Phytomedicine Plus* (2023), doi: <https://doi.org/10.1016/j.phyplu.2023.100419>

This is a PDF file of an article that has undergone enhancements after acceptance, such as the addition of a cover page and metadata, and formatting for readability, but it is not yet the definitive version of record. This version will undergo additional copyediting, typesetting and review before it is published in its final form, but we are providing this version to give early visibility of the article. Please note that, during the production process, errors may be discovered which could affect the content, and all legal disclaimers that apply to the journal pertain.

© 2023 The Author(s). Published by Elsevier B.V.
This is an open access article under the CC BY-NC-ND license (<http://creativecommons.org/licenses/by-nc-nd/4.0/>)

Integrated network pharmacology and *in-silico* approaches to decipher the pharmacological mechanism of *Selaginella tamariscina* in the treatment of non-small cell lung cancer

Sunil Kumar^a, Faheem Abbas^b, Iqra Ali^c, Manoj K. Gupta^d, Saroj Kumar^e, Manoj Garg^f, Deepak Kumar^{a*}

^aDepartment of Pharmaceutical Chemistry, School of Pharmaceutical Sciences, Shoolini University, Solan-173229, Himachal Pradesh, India.

^bKey Lab of Organic Optoelectronics and Molecular Engineering of Ministry of Education, Department of Chemistry, Tsinghua University, Beijing 100084, PR China.

^cDepartment of Biosciences, COMSATS University Islamabad, Islamabad Campus, Pakistan.

^dDepartment of Chemistry, School of Basic Sciences, Central University of Haryana, Mahendergarh, H.R., 123031, India.

^eDepartment of Biophysics, All India Institute of Medical Sciences, New Delhi, India.

^fAmity Institute of Molecular Medicine and Stem Cell Research, Amity University UP, Sector-125, Noida 201313, India.

*Corresponding author at:

Dr. Deepak Kumar

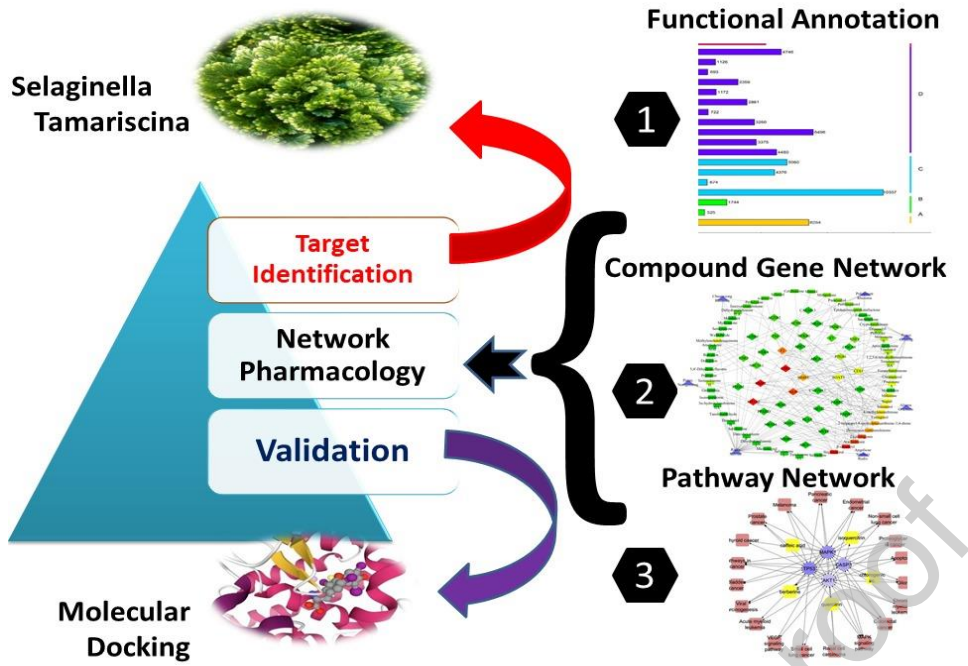
Professor, Department of Pharmaceutical Chemistry, School of Pharmaceutical Sciences, Shoolini University, Solan-173229, Himachal Pradesh, India.

E-mail address: guptadeepak002@gmail.com

Highlights

- Network pharmacology uncovered the pharmacological mechanism of active phytochemicals from *Selaginella tamariscina* in the treatment of non-small cell lung cancer (NSCLC).
- *In-silico* molecular docking studies revealed that active phytochemicals of *Selaginella tamariscina* may be useful for the treatment of NSCLC.
- Molecular dynamics simulations studies demonstrated that isocryptomerin demonstrates the best interactions and affinities with the potential anticancer targets.
- The density functional theory (DFT) reveals the effectiveness of seven phytochemicals of *Selaginella tamariscina* for the treatment of NSCLC.
- ADME analysis of the seven potential phytochemicals demonstrated drug-like properties.
- Toxicity predictions of the screened phytochemicals had an acceptable toxicity profile.

Graphical Abstract



Abstract

Background and purpose

Non-small cell lung cancer (NSCLC) is a major pathological type of lung cancer and accounts for more than 80% of all cases. In healthcare management, it is challenging to understand the mechanism of NSCLC due to diverse spectra and the limited number of reported data. *Selaginella tamariscina* is an evergreen perennial plant, hermaphrodite, and used to treat numerous diseases, including NSCLC. In vitro research revealed the therapeutic importance of *S. tamariscina* in contrast to NSCLC, but the molecular mechanism is still unclear. In the present study, a network pharmacology technique was employed to uncover the active ingredients, their potential targets, and signaling pathways in *S. tamariscina* for the treatment of NSCLC.

Methods

Putative ingredients of *S. tamariscina* and significant genes of NSCLC were retrieved from the public database after screening. The overlapped targets among *S. tamariscina* related compounds and NSCLC were predicted using Venn plot. Following that, a compound-target-disease network was constructed using Cytoscape to decipher the mechanism of *S. tamariscina* for NSCLC. KEGG pathway and GO enrichment analysis were performed to investigate the molecular mechanisms and pathways related to *S. tamariscina* for NSCLC treatments. Lastly, molecular docking and molecular dynamic simulation analysis were performed to validate the interaction that exists between compounds and target proteins.

Results

The findings of the current analysis explored the compound–target–pathway network and figured out that Hinokiflavone, Heveaflavone, Neocryptomerin, Isocryptomerin, Apigenin, Sotetsuflavone, and Cryptomerin B decisively contributed to the development of NSCLC by affecting AKT1, EGFR, VEGFA, and GSK3B genes. Later, molecular docking and simulation analysis was conducted to validate the successful activity of the active compounds against potential targets. Lastly, it is concluded that predicted multi-target compounds of *S. tamariscina* will help in improving the body's sensitivity to NSCLC by regulating the expression of AKT1, EGFR, VEGFA, and GSK3B, which may act as potential therapeutic targets of NSCLC.

Conclusion

Integrated network pharmacology and docking analysis revealed that *S. tamariscina* exerted a promising preventive effect on NSCLC by acting on diabetes-associated signaling pathways. The current findings propose that AKT1, VEGFA, EGFR, and GSK3B genes are promising and viable therapeutic targets to reduce the incidence of NSCLC, thereby exerting potential therapeutic effects in NSCLC. This approach introduces a groundwork for further research on the protective mechanisms of *S. tamariscina* for NSCLC and applications of network pharmacology in drug discovery.

Keywords: *Selaginella Tamariscina*, Network Pharmacology, Non-small cell lung cancer, Phytochemicals, Molecular docking, ADME

Abbreviations: ADME, Absorption, distribution, metabolism, and excretion; BP, Biological process; BBB, Blood–brain barrier; CC, Cellular component; DL, Drug-likeness; DFT, Density functional theory; DOS, Density of state analysis; DAVID, Database for annotation, visualisation, and integrated discovery; EGFR, epidermal growth factor receptors; FMOs, Frontier molecular orbital analysis; HOMO, Highest occupied molecular orbital; LUMO, Least unoccupied molecular orbital; MD, Molecular dynamics; MEP, Molecular electrostatic potential; MF, Molecular function; MMGBSA, Molecular mechanics with generalised Born and surface area solvation; NP, Network pharmacology; NSCLC, Non-small cell lung cancer; OB, oral bioavailability; OMIM, Online Mendelian Inheritance in Man; PPI, Protein-protein interaction; STRING, Search Tool for the Retrieval of Interacting Genes; SCLC, Small cell lung cancer; TCMID, Traditional Chinese Medicine Integrated Database; TCMSP, Traditional Chinese Medicine Systems Pharmacology;

1. Introduction

Lung cancer is the leading cause of cancer-related deaths, worldwide. Non-small cell lung cancer (NSCLC) is distinguished from small cell lung cancer (SCLC) (Madeddu et al., 2022). There are more than 50 distinct histological subtypes. For example, NSCLC is subdivided into large-cell carcinoma, squamous-cell carcinoma, and adenocarcinoma (Chaft et al., 2022). In 2020, lung cancer will be the major cause of cancer-related death, accounting for 1.8 million deaths (Pan et al., 2022). Lung cancer is the second most often diagnosed malignancy worldwide, accounting for both sexes. Despite recent therapeutic advancements brought about by the introduction of targeted therapy and immunotherapy, 5-year survival rates remain dismal (10–20%). NSCLC continues to be one of the most prevalent cancers in the globe (Huber et al., 2022). Historically, several risk factors have been linked to the development of NSCLC, including smoking, air pollution, occupational exposure, radiation, radon, and asbestos (Burzić et al., 2022). In recent years, a variety of systemic treatments for NSCLC patients have emerged, including immunotherapy (as monotherapy or in combination with other anticancer medicines) and targeted therapies (Wang et al., 2022). NSCLC accounts for around 85% of all lung cancer diagnoses and, over the past ten years, the incidence rate has remained stable (Aregui et al., 2022). In this context, a rising number of activating oncogene mutations have been found: the KRAS (20–30%), EGFR (10–15% of Caucasian individuals and up to 40% of Asian patients), and ALK (anaplastic lymphoma kinase) genes are the most prevalent. In 3–5% of NSCLC patients (Rekowska et al., 2022), the Echinoderm Microtubule-associated protein Like 4 gene is involved in an ALK translocation, which accounts for the majority of ALK gene rearrangements (EML4). This molecular rearrangement produces a fusion protein with constitutive kinase activity that constantly promotes cell proliferation and survival and prevents apoptosis by regulating intracellular signalling pathways (Lei et al., 2022).

The past decade of research in the field of molecular biology has significantly advanced the understanding of the molecular pathways underlying the development and progression of NSCLC (Cao et al., 2022). This has allowed great progress in the development of therapeutic methods for NSCLC, which accounts for 84% of all lung malignancies (Balasundaram et al., 2022). Despite recent advances in treatment methods, lung cancer continues to be the top cause of cancer-related deaths worldwide, representing 13% of all cancer-related fatalities (Kennedy et al., 2022). Pharmacotherapy consisting of natural products is seen as a viable therapeutic method for NSCLC and could provide answers to the questions raised above. Traditionally, several plant species, including *Platycodon grandiflorum*, *Perilla frutescens*, *Tussilago farfara*, *Drabane morosa*, *Stemona japonica*, *Prunus armenica*, *Rhus verniciflua*, and *Morus alba* are used to cure various lung diseases including cancer (Mlilo and Sibanda, 2022). It has been claimed that medicinal plants contain natural scaffolds in form of that help in the treatment of lung cancer, metastasis, apoptosis, involving cancer progression, and multidrug resistance (Motallebi et al., 2022). Numerous phytochemicals are included in (Table 1) below that have been shown to have considerable antiproliferative, apoptotic, and anti-metastatic effects against lung cancer (Ibrahim et al., 2022). In the future, utilizing innovative approaches, and the advantages of phytochemicals in cancer therapy may be helpful in the treatment of people who have lung cancer (Tuorkey, 2015).

S. tamariscina is a traditional medicinal plant for the treatment of some advanced cancers in the Orient. Previous investigation has shown that the chemical components of Selaginella plants mainly include flavonoids, selaginellins, lignans, and sterols (Lin et al., 2000) (Wen et al., 2021) (He et al., 2019) (Gao et al., 2007) which have such pharmacological effects as anticancer, anti-virus and anti-inflammatory. The findings of this study show that *S. tamariscina* is a root and distinctive source of numerous promising phytochemicals, making it a valuable and adaptable plant with a wide range of therapeutic qualities.

Network pharmacology (NP) is a rising star in the field of drug discovery, as it integrates systematic medicine with information science (Noor et al., 2022b). It is an integrative *in-silico* approach for introducing a 'protein-compound/disease-gene network in order to reveal the mechanisms underlying the synergistic therapeutic actions of traditional medicines (Batool et al., 2022) (Noor et al., 2022a). This advancement, in turn, has shifted the paradigm from a 'one-target, one-drug' mode to a 'network-target, multiple-component-therapeutics' mode.

This study provides novel insight to understand the network pharmacology-based approach to identifying *S. tamariscina* active phytochemicals for the treatment of liver cancer. *S. tamariscina* bioactive compounds with their anti-cancer effect were analyzed by using the network pharmacology along with molecular-docking and simulation approaches, which sparked the attention towards the search for candidate drugs from this plant. Moreover, further wet lab experiments are needed to explore the compound's pharmacological potential.

2. Materials and methods

2.1 Collection and screening of active compounds

The information on active compounds of *S. tamariscina* was retrieved from the literature as well as databases of biologically active phytoconstituents including Indian Medicinal plants, Phytochemical from, Therapeutics databases (IMPPAT) (Mohanraj et al., 2018), Traditional Chinese medicine systems pharmacology (TCMSP) (Ahmed and Ramakrishnan, 2012) (Xu et al., 2012), and KNApSAcK (Shinbo et al., 2006). The literature search was carried out using the keywords " *Selaginella tamariscina* " on Pubmed and Google Scholar, respectively. The chemical structures of the active compounds were obtained from PubChem (Kim et al., 2016a) and ChemSpider (Pence and Williams, 2010). The active constituents which retained $OB \geq 30\%$ and $DL \geq 0.18$ values were considered novel compounds and selected for further analysis. Moreover, the information about chemical ID, Molecular weight, and canonical smiles of active compounds was obtained from PubChem (Kim et al., 2016b). Following that, Molsoft (James et al., 2015) and SwissADME (Daina et al., 2017) were used to compute the DL and OB of all active ingredients as shown in (Fig. 1).

2.2 Target gene screening

The potential targets of *S. tamariscina*-related compounds were retrieved by using Swiss target prediction tool. To attain this goal, screened compounds were uploaded to SwissTarget prediction and STITCH (Szklarczyk et al., 2016) databases with a search limited to '*Homo sapiens*'. The SMILES of predicted compounds were inputted in Swiss Target Prediction to acquire targets using the reverse pharmacophore matching approach. Only targets with a combined score of less than 0.7 were chosen for further research. Consequently, the targets with a chance of 0.7 were chosen (Gfeller et al., 2014). Similarly, active constituents were obtained from the STITCH database by choosing *Homo sapiens* as the species, and targets with ≥ 0.7 combined scores were retained.

The next preliminary phase in exploring the molecular mechanisms of herbal drugs to cure various diseases and disorders is the forecasting of disease-related genes. With the terms 'Non-Small Cell Lung Cancer' two databases-Gene Card (Safran et al., 2010) and Online Mendelian Inheritance in Man (OMIM)-were searched to find genes associated with the diseases. These databases provide brief genomic data and functional annotation for well-known human genes. The final gene list was purged of duplicated genes, and the standard name of the target gene was retrieved from UniProtKB (Boutet et al., 2007), having the organism chosen to be '*Homo sapiens*'. After that, a Venn diagram was created to identify the common targets between *S. tamariscina* and NSCLC. These targets were later considered key targets.

2.3 Pathway and functional enrichment

Gene enrichment and KEGG pathway analysis were performed using Database for annotation, visualisation, and integrated discovery (DAVID) (Huang et al., 2007). DAVID was used to perform functional annotation on a list of important genes at three different levels: cellular component (CC), molecular function (MF), and biological process (BP). The functional enrichment database DAVID, which is accessible online, aids researchers in understanding the activity of a large number of genes. In the present research, p-values < 0.01 were chosen, and the top 10 KEGG pathways and GO enrichments were selected for further analysis.

2.4 Network constructions

A network analysis was done to understand the mechanism of *S. tamariscina* in lung cancer. Cytoscape 3.8.0, is a publicly downloadable graphical user interface for visualization and interpretation of biomolecular interaction networks (Smoot et al., 2011). In the current study, Cytoscape 3.8.0 was used for network construction and interpretation. In the network, nodes represent the active components and target genes, and edges depict interactions between active components and their target genes. Furthermore, the topological methods of Cytoscape 3.8.0 were used for the identification of key genes. A total of 11 topological methods are available among which degree, a topological attribute that shows the significance of a compound/target gene/pathways in a network diagram, was calculated using a network analyzer program. Furthermore, "important targets" were defined as target genes with significant linkage.

2.5 Protein-protein network construction

The protein-protein interaction network of target genes was created by using an online STRING database (<https://string-db.org/>) (Mering et al., 2003), and "*Homo sapiens*" was selected as the organism. Genes with ≥ 0.5 combined score were retained for further investigation and the network was imported in Cytoscape 3.8.0. A plugin CytoHubba was used to identify and analyze core regulatory genes considered "hub genes". CytoHubba is an interface used to analyze as well as visualize networks by using different eleven methods of scoring. Hub genes are those that have the highest degree based on interactions.

2.6 Molecular docking analysis

2.6.1 Structure retrieval

The phytochemicals structures of active compounds were retrieved from the PubChem data base (<https://pubchem.ncbi.nlm.nih.gov>) (Kim et al., 2016a). Similarly, the X-ray crystallography-based structure of targets was obtained from RCSB Protein Data Bank (PDB) (<https://www.rcsb.org/>) (Kouranov et al., 2006). Receptor ligands interaction was studied for selected phytochemicals on different crystallographic receptors as anticancer targets, their absorption, distribution, metabolism, and excretion (ADME), and toxicity profile

predicted. The best ligand-protein complex was selected based on the best dock score and subjected to Molecular Dynamic (MD) simulation at 200ns (Klepeis et al., 2009).

2.6.2 Target and ligand preparation

The retrieved structures of the phytochemicals Hinokiflavone, Heveaflavone, Neocryptomerin, Isocryptomerin, Apigenin, Sotetsuflavone, and CryptomerinB docked against four different crystallographic receptors as anticancer targets AKT1, Crystal Structure of Human AKT1 having PDB ID: 3O96, VEGFA, the crystal structure of human VEGF-A receptor binding domain having PDB ID: 4KZN, EGFR, Epidermal Growth Factor Receptor tyrosine kinase domain having PDB ID: 1M17 GSK3B, the crystal structure of GSK3B having PDB ID: 5HLP receptor. The mutations, resolution, missing regions, and active state of the five different PDB structures are given in the supporting data (**Table S1**). All water molecules and ions were deleted, hydrogen atoms were added and the energy of the system was minimized with AutoDock Tool 1.5.7 version (Nguyen et al., 2020). After the target preparation, the next step was to prepare the ligands for molecular docking on the selected four different crystallographic receptors. All the structures of the phytochemicals were converted into .sdf format by using Open Babel GUI, and .sdf format of all phytochemicals were subjected for energy minimization and converted to .pdbqt format in the PyRx free version before molecular docking (Tanveer et al., 2021).

2.6.3 Molecular docking studies

In structural molecular biology and computer-assisted drug design, one of the most important tools is called molecular docking (Zochedh et al., 2022). The purpose of ligand-protein docking is to make predictions about the predominant binding modes of a ligand to a protein whose three-dimensional structure is already known (Dilshad et al., 2022). Effective docking techniques quickly search high-dimensional spaces with a scoring function that ranks potential dockings accurately (Dhameliya et al., 2022). Docking has the ability to do virtual screening on enormous chemical libraries, rate the results, and suggest structural theories for how the ligands suppress the target, which is crucial for lead refinement (Oyedele et al., 2022). To find the binding interactions of all the phytochemicals in the active sites of four different crystallographic receptors as anticancer targets having PDB ID: 3O96, 4KZN, 1M17, and 5HLP prior to molecular docking, all water and ions were removed from the retrieved crystal structure, while the nonpolar hydrogens were merged. Then, the protein was minimized and optimized through AutoDock Tool 1.5.7 version (Jumbo et al., 2022), bundled with the MGLTools package (version 1.5.6) to add charges, polar hydrogen atoms, and set up rotatable bonds (CHEBAIBI et al., 2021). The molecular docking was performed using AutoDock Vina v1.1.2 version (Shakil, 2021) in PyRx free version (Syarafina et al., 2022). The docking scores were resulted in the generated .CSV file. The output docking scores were defined as affinity binding (Kcal/mol). After the molecular docking, analyzed the best poses having interactions by using the Discovery Studio version v21.1.0.20298 (Naeem et al., 2022). Default docking algorithms were used, and coordinates for PDB ID: 3O96 [X=7.8, Y= -11, Z=19],

1M17 [X= 10.9, Y= 7.8, Z= 54.06], 5HLP [X=0.93, Y=25.92, Z=-16.43], and 4KZN [X=6.55, Y=-5.22, Z=-0.65] were set in the grids along with the standard size and placed in active site pocket center. The lowest binding energies were the best suitable for interactions.

2.7 ADME and drug likeliness analysis

ADME properties enable drug researchers in determining the safety and effectiveness of a medication and are crucial for FDA approval (Li, 2001). It is essential to acquire human pharmacokinetic data for the discovery and development of new drugs and the proper delivery of pharmaceuticals (Selick et al., 2002). The virtually screened phytochemicals from *S. tamariscina* acquired with the use of dock scores were then submitted to ADME analysis. SwissADME (<http://www.swissadme.ch>) (Daina et al., 2017) and ADMET 2.0 online servers (<https://admetmesh.scbdd.com>) (Xiong et al., 2021) tools accessed on 10 October 2022 were used to estimate drug-likeness and ADME features of phytochemicals. Lipinski's criteria were used to determine only when the initial phytochemicals from *S. tamariscina* screened were suitable for docking. Any phytochemicals that failed to meet two of Lipinski's criteria were deemed unsuitable for further evaluation. Other than Lipinski's criteria, physicochemical assessment and drug-like abilities of all the selected phytochemicals were also considered during the ADME screening process (Chandran et al., 2022).

2.8 Toxicity analysis of the phytochemicals

Assessment of phytochemical's toxic effects and effectiveness is critical to drug research and development because drug-induced toxicities in the kidneys, brain, liver, heart and contribute to about 75 % of current drug retention and discontinuation (Cooper, 2016). After the ADME and drug likeliness analysis of the phytochemicals from *S. tamariscina* were selected for toxicity prediction by using *in-silico* methods, and toxicity investigation was evaluated with the use of the OSIRIS property explorer (<http://www.organic-chemistry.org/prog/peo>) tools accessed on 12 October 2022 (Agrawal et al., 2022) and ADMET 2.0 online servers (<https://admetmesh.scbdd.com>) (Xiong et al., 2021) tools accessed on 12 October 2022, were used to predict the toxicity features of the phytochemicals.

2.9 MMGBSA analysis

After docking, MMGBSA analysis was performed for the best-selected compound Isocryptomerin fit in target protein AKT1 (PDB ID: 3O96) by Prime Schrodinger. MMGBSA, the most powerful and quickest force field approach estimates the relative binding affinity of the protein-ligand complex in Kcal/mol to calculate van der Waals, covalent, generalized born electrostatic, nonpolar, and Coulombic energies to check the stability of protein-ligand complex throughout the simulation to validate the docking results (Zhang et al., 2017). The docking output file was used as input for MMGBSA, then minimizing the energy of the docking pose, and calculating binding free energies of the complex using generalized born surface area.

2.10 Molecular dynamics simulation

To study protein-ligand interactions under physiological conditions, 200 ns MD simulation of best-selected complex was conducted via Desmond (Blessy and Sharmila, 2015). For MD simulation, the complex was preprocessed with default settings and removed steric clashes, bad contacts, and distorted geometries via Maestro (Madhavi Sastry et al., 2013). TIP3P was selected as the solvent model and 10Å orthorhombic box was chosen (Shivakumar et al., 2010). During water equilibration, the kinetic and potential energy of the complex fluctuates while total energy remains the same. System was prepared via the system builder tool while neutralized by introducing 0.15M NaCl salt at 310K temp. and 1 atm pressure during simulation (Rasheed et al., 2021). Lastly, trajectories saved and computed all essential analyses to determine the stability of protein and ligand complex throughout time.

2.11 Density functional theory (DFT)-analysis

For all molecules, the investigation was carried out computationally using the Gaussian 16 (Tromer et al., 2021) and Gauss View 06 package (Haghi et al., 2022). It was decided to use the B3LYP (Hertwig and Koch, 1997) functional with the basis set 6-31G** for all of the compounds that were reported. The theoretically calculated coordinates of all of the designed molecules can be found in the attached supplementary information (**Table S2**). To obtain the energy gap values, the same DFT and TD-DFT method (Obot et al., 2015) was employed to locate the lowest energy levels up to the sixth n states for the geometry optimization. All other properties like frontier molecular orbital analysis (FMOs) (Chen and Solomon, 2002), molecular electrostatic potential (MEP) (Suresh et al., 2022), and density of state analysis (DOS) (Fung et al., 2021) been performed using the same level of theory.

3. Results

3.1 Screening of active compounds and targets

After screening, and filtering, a total of active seven phytochemicals of *S. tamariscina* with parameters having $DL \geq 0.18$ and $OB \geq 30\%$ were selected. Oral Bioavailability (OB) is the rate and extent to which the active constituent or active moiety of a drug is absorbed from a drug product and reaches circulation. Compounds that are formulated to have high bioavailability will be more effective, as they will help the body to absorb more of the appropriate nutrient without having to take higher doses. Drug likeness (DL) computes the likelihood of a molecule being bioavailable as an oral drug. Furthermore, the Swiss Target Prediction database yielded 148 possible target genes for seven active components. Once the drugs promising targets were determined, 5804 target genes related to NSCLC were extracted from the Gene Cards and OMIM databases. Later, a Venn diagram demonstrated a total of 148 putative anti-cancer genes were chosen and referred to as key targets; the results obtained are shown in (**Table 2**).

3.2 Compounds target network constructions

The network diagram for the "active compound-targeted genes " was created using seven active compounds, and 1500 targets with the highest number of related genes. Each of these active substances has several targets, demonstrating that when *S. tamariscina* is employed as an anti-NSCLC cancer drug, these targets result in a synergistic effect. The degree of these seven phytochemical compounds in the compound-target network pathway was assessed to highlight the compounds having the highest degree in "Compound-target" network. Current findings revealed that flavonoids have a comparatively maximum degree than other classes of compounds (**Table 3**).

3.3 PPI network construction

To create a PPI network, 149 overlapped genes were submitted to the STRING database. Nodes and their connected relationships in the PPI network show the interactions among several targets during the development of disease (**Fig. 2A**). Afterward, a network analysis tool evaluated the PPI network of overlapping genes (**Fig. 2C**). The highest levels of overlapping were observed in AKT1 (168), VEGFA (156), EGFR (134), ESR (126), SRC (124), PTGS2 (112), MMP9 (100), PPARG (90), KDR (66), and GSK3B (64) (**Fig. 2D**). The highest degree indicates that the targeted genes strongly correlate with one another; as a result, all of these genes may be important targets. Four genes, specifically AKT1, VEGFA, EGFR, and GSK3B, were chosen for molecular-docking studies since they were found to be *S. tamariscina* primary NSCLC targets as shown in (**Table 4**).

3.4 Go and KEGG analysis

The potential biological roles of *S. tamariscina* targets were revealed by the functional annotation and enrichment analysis. *S. tamariscina* targets were enriched in multiple processes including protein autophosphorylation, positive regulation of gene expression, the extracellular exosomes, and other things (**Fig. 3**). To determine the important signaling pathways connected to *S. tamariscina* anti-NSCLC action, the KEGG pathway analysis was carried out. It is noteworthy that the majority of the genes were associated with the pathways for lung cancer. Last but not least, KEGG pathway analysis showed that the genes AKT1, VEGFR, EGFR, and GSK3B were considerably enriched in disease-related pathways (**Fig.4**). The molecular mechanism of the tested phytochemicals on the targeted genes AKT1, VEGFR, EGFR, GSK3B, and compounds regulating these genes, how they reduce the risk of cancer shown in the (**Fig. 5**).

3.5 Molecular docking analysis

3.5.1 Virtual screening on anticancer targets

Molecular docking analysis was performed among compounds (Hinokiflavone, Heveaflavone, Neocryptomerin, Isocryptomerin, Apigenin, Sotetsuflavone, and CryptomerinB) and target proteins to investigate and compare the binding energies and interactions with the selected target. The best affinity scores of phytochemicals for PDB ID: 3O96, 1M17, 5HLP, and 4KZN were observed as -14.1, -9.9, -9.8, and -7.7, while the standard drug has a maximum score of -13.9, -6.7, -8.3, and -3.5, kcal/mol respectively. Isocryptomerin demonstrated the highest binding affinity -14.1 and reference molecule -13.9 kcal/mol for (PDB ID: 3O96) when it is compared to the standard inhibitor and other crystallographic receptors. The docking poses of the isocryptomerin with the highest binding affinity receptor (PDB ID: 3O96), analyzed with 2D interactions as shown in the figures given below the types of contacts formed (**Fig. 6**) showing the types of interactions formed between isocryptomerin and crystallographic receptors as anticancer targets (PDB ID: 3O96). The binding affinity scores of isocryptomerin along with the reference molecule and other crystallographic receptors (**Table 5**). Hinokiflavone shows the highest binding affinity -9.9 and reference molecule -6.7 kcal/mol for (PDB ID: 1M17) when it is compared to the reference molecules and other crystallographic receptors. The docking poses of the hinokiflavone with the highest binding affinity receptor (PDB ID: 1M17) were analyzed with 2D interactions as shown in (**Fig. 7**), showing the types of interactions formed between hinokiflavone and crystallographic receptors as anticancer targets (PDB ID: 1M17). The best affinity scores of hinokiflavone along with the reference molecule for (PDB ID: 1M17) (**Table 6**). Sotetsuflavone reveals the highest binding affinity -9.8 and reference molecule -8.3 kcal/mol for (PDB ID: 5HLP) when it is compared to the reference molecules and other crystallographic receptors. The docking poses of the sotetsuflavone with the highest binding affinity receptor (PDB ID: 5HLP), were analyzed using 2D interactions as shown in (**Fig. 8**), a diagram showing the types of bonding established between sotetsuflavone and crystallographic receptors as anticancer target (PDB ID: 5HLP). The best affinity scores of sotetsuflavone along with the reference molecule for (PDB ID: 5HLP) are given in (**Table 7**). Isocryptomerin demonstrated the highest binding affinity -7.7 and reference molecule -3.5 kcal/mol for (PDB ID:4KZN) when it is compared to the reference molecules and other crystallographic receptors. The docking poses of the isocryptomerin with the highest binding affinity receptor (PDB ID: 4KZN) were analyzed with 2D interactions (**Fig. 9**) diagram showing the types of interactions formed between crystallographic receptors as anticancer target (PDB ID: 4KZN). The best affinity scores of isocryptomerin along with the reference molecule for (PDB ID: 4KZN) (**Table 8**). The hydrogen bonding interaction is crucial for better interaction with the receptor active sites. In the reference molecule, only two hydrogen bonding interactions are formed with the residues Cys 773 and Asp 831. Isocryptomerin demonstrating hydrogen bonding interaction with one new residue Tyr 272 and a reference molecule was found to be interacted residue Arg 273 with (PDB ID: 3O96). Hinokiflavone showed hydrogen bonding interaction with four new residues Arg 817, Asn 818, Asp

831, Glu 734 whereas in the reference molecules only one hydrogen bonding interaction was found with residue Met 769 in the (PDB ID: IM17). Sotetsuflavone has hydrogen bonding interaction with two similar residues Asp 133, Val 135 and in the reference molecules, similar hydrogen bonding interactions were observed with these residues Asp 133, Val 135 in the (PDB ID: 5HLP). Isocryptomerin reveals hydrogen bonding interaction with one new residue Cys 104 where as in the reference molecule has hydrogen bonding with Cys 68 in the (PDB ID: 4KZN). Four new hydrogen bonding founds in the phytochemicals with residues Arg 817, Asn 818, Asp 831, Glu 734 which are crucial for the activity as shown in (**Table 9**). The binding affinity of the docked molecule with target proteins is elaborated in (**Fig. 10**).

3.6 ADME and drug likeliness

After docking analysis, the phytochemicals Hinokiflavone, Heveaflavone, Neocryptomerin, Isocryptomerin, Apigenin, Sotetsuflavone, and Cryptomerin B from the plant *S. tamariscina* were selected for the ADME analysis based on the best dock score with four different crystallographic receptors as anticancer targets. Hinokiflavone was indicated to have four rotatable bonds ten H-bond acceptors five H-bond donors along with a synthetic accessibility score of 4.05, a bioavailability score of 0.55 predicted and ligand demonstrated low GI absorption with no BBB permeation. Heveaflavone was demonstrated to have six rotatable bonds ten H-bond acceptors three H-bond donors along with a synthetic accessibility score of 4.6 and demonstrated low GI absorption along with a bioavailability score of 0.55. It is found to have no BBB permeation. Neocryptomerin was found to have ten H-bond acceptors four H-bond donors along with five rotatable bonds and has synthetic accessibility score of 4.21, demonstrated low GI absorption with a bioavailability score of 0.55, Neocryptomerin showing no BBB permeation in the ADME analysis. Isocryptomerin has ten H-bond acceptors four H-bond donors along with five rotatable bonds and has a synthetic accessibility score of 4.21. Isocryptomerin shows low GI absorption with a bioavailability score of 0.55 and has no BBB permeation properties. Apigenin was demonstrated to have five H-bond acceptors, and three H-bond donors along with one rotatable bond and has a synthetic accessibility score of 2.96, Apigenin was found to have high GI absorption with no BBB permeation and shows a bioavailability score of 0.55. Sotetsuflavone has ten H-bond acceptors, five H-bond donors along with four rotatable bonds, and has a synthetic accessibility score of 4.37, Sotetsuflavone was found to have low GI absorption with no BBB permeation and demonstrates a bioavailability score of 0.55. Cryptomerin B was found to have six rotatable bonds ten H-bond acceptors three H-bond donors along with a synthetic accessibility score of 4.33, a bioavailability score of 0.55 predicted and ligand demonstrated low GI absorption with no BBB permeation. The preliminary ADME screening was focused primarily on Lipinski's rule of five, gastrointestinal retention properties, and PAINS. The phytochemicals following Lipinski's rule of five, with strong gastrointestinal retention characteristics and no PAINS signals, were identified for screening. For the seven phytochemicals screening was performed based on Lipinski's rule of five, synthetic accessibility score, and PAINS analysis, gastrointestinal retention property, and other criteria of druggability were considered. The phytochemicals following Lipinski's rule of five,

exhibiting gastrointestinal retention properties and reproducing synthetic accessibility scores less than five along with zero PAINS alerts, were identified as shown in (Table 10). The ADME analysis for all seven phytochemicals from the plant *S. tamariscina* is shown in (Fig. 11).

3.7 Toxicity-based screening

After ADME analysis next step was to investigate the toxicity profile of the virtually screened ligands. The phytochemicals were selected on the basis of docking score with crystallographic receptors of anticancer targets having PDB ID: 3O96, 4KZN, 1M17, and 5HLP. The phytochemicals Hinokiflavone, Heveaflavone, Neocryptomerin, Isocryptomerin, Apigenin, Sotetsuflavone, and Cryptomerin B were selected for toxicity profile prediction. The phytochemicals from *S. tamariscina* Hinokiflavone demonstrated no indication for mutagenic effect, no tumorigenic risk found, no irritant property observed, and mild reproductive effects. Heveaflavone was found to have no tumorigenic risk, no irritant properties along with no reproductive effects, and no mutagenic indication. Neocryptomerin shows no mutagenic indication, no tumorigenic risk, no irritant property, and has mild reproductive effects. Isocryptomerin revealed no mutagenic indication, no tumorigenic risk, no irritant properties, and mild reproductive effects. Apigenin shows no mutagenic indication, no tumorigenic risk, no irritant properties, and no reproductive effects. Sotetsuflavone demonstrated no mutagenic indication, no tumorigenic risk, no irritant properties, and no reproductive effects. Cryptomerin B indicated no mutagenic indication, no tumorigenic risk, no irritant property, and mild reproductive effects. and finally, Isocryptomerin had acceptable toxicity and druggability profiles all of them, therefore was chosen as the final hit compound for MD-simulations analysis. The prediction probability values are transformed into six symbols: 0-0.1(---), 0.1-0.3(--), 0.3-0.5(-), 0.5-0.7(+), 0.7-0.9(++), and 0.9-1.0(+++) as shown in (Table 11).

3.8 MMGBSA-binding free energy calculations

The computational cost-effective technique MMGBSA is used to compute the binding free energy of ligand in contact with the protein. Prime Schrödinger provides a detailed energy profile of protein and ligand complex as it computes coulombic (-12.92), covalent (2.95), lipophilic (-6.50), van der Waals (-19.01), hydrogen bonding (-1.08) and the total binding free energy is -34.52 for Isocryptomerin. Lower binding free energy (more negative values) denoted stability and favorable binding of ligand at the active site of the target protein. According to binding free energy values, coulombic energies (-12.92) contribute more than others. Prime MM-GBSA evaluates binding energy calculations more accurately than molecular docking and reveals stronger binding of the ligand to the receptor (Pattar et al., 2020). The MMGBSA-binding free energy calculations are shown in (Fig. 12).

3.9 Molecular dynamics simulation

A 200ns MD simulation was conducted for the best complex to compute RMSD, RMSF, protein-ligand contents, and some other parameters from MD trajectories with reliable findings. **(Fig. 13)** illustrate that how RMSD of protein in contact with ligand fluctuates over time and it's a crucial way to validate the accuracy and stability of docking geometry. Protein RMSD reaches stability at 5ns and fluctuates within 4 Å up to 135ns. The structure of AKT1 slightly growing and there was a minor increase in RMSD at 136ns within the satisfactory range throughout the time. The average protein RMSD value is 2.4 to 5.6 Å and the structure remains stable throughout the simulation. RMSD of ligand fit to protein stable at 2ns till 40ns within the range of 1 to 2.5 Å and then there is an abrupt increase in ligand RMSD within the range of 3 to 4.8 Å that represents interaction with AKT1. After that, there is some decrease in ligand RMSD from 100 to 200ns simulation within the range of 1.6 to 3 Å. At some points, ligand RMSD increases and decreases abruptly due to rotatable bonds while no significant changes indicate that ligand is stably bound in the active site of AKT1 protein. **(Fig. 14A and 14B)** demonstrate atom-wise RMSF value of Isocryptomerin and residue-wise RMSF value of AKT1 protein respectively. The majority of amino acid residues have RMSF value <3.7 Å except for one higher peak in the middle and N and C terminal variations indicate the presence of loops regions while areas with minimum fluctuations represent alpha helixes and beta strands and contribute to the rigidity of protein structure. Isocryptomerin maintains RMSF value within 1.20 to 1.75Å for the majority of atoms with respect to protein.

(Fig. 15) depicts numerous forms of protein-ligand interactions including hydrogen, ionic bonds, hydrophobic contacts, and water bridges that occur during MD simulation, and values above 1.0 are considered feasible. Asn54, Glu85, Tyr272 are important for hydrogen bonds and water bridges. Trp80, Val83, Arg273 residues make hydrophobic interactions while the most representative ionic bonds are formed by Thr160 and Lys297 residues. **(Fig. 16)** top panel demonstrates the total number of protein-ligand interactions whereas the lower panel displayed residues that come into contact with ligand. Asn54, Trp80, Glu85, Thr160, Arg273, Asp274 residues make more than one specific contact with Isocryptomerin and occur for more than 30% of simulation time and are represented by a darker shade of orange **(Fig. 17)**. Torsion plot of Isocryptomerin find out conformation of all 9 rotatable bonds throughout the simulation. The left panel shows 2D schematic of Isocryptomerin with color-coded rotatable bonds while the right panel shows a dial plot and bar plots of the same color and values expressed in kcal/mol. Histogram and torsion potential relationships give insights that Isocryptomerin maintains protein-bound conformation **(Fig. 18)** Ligand properties i.e., Molecular surface area (MolSA) 76 Å, solvent accessible surface area (SASA) 120Å, Radius of Gyration (rGyr) 30Å, polar surface area (PSA) 295Å are within the optimum range. The isocryptomerin properties were determined via MD simulation **(Table 12)**.

3.10 Frontier molecular orbital analysis (FMOs)

All density functional theory (DFT) analyses were carried out using the hybrid functional B3LYP (Civalleri et al., 2008) at basis set 6-31G (d, p). The electron density of HOMO and LUMO can be easily understood by FMOs model. The distribution pattern of charges in LUMO (lowest unoccupied molecular orbital) and HOMO (highest occupied molecular orbital) can be estimated using frontier molecular orbitals. Frontier molecular orbitals, also known as HOMO and LUMO, are quantum computational methods for predicting chemical reactivity and stability based on the highest and lowest excited states. The degree to which an electron is excited from its lowest ground state to its excited state is the primary factor that determines electronic absorption as well as the energy gap between orbitals (Saravanan and Balachandran, 2014). It is important to consider the energy gap between two states, known as HOMO and LUMO, when determining which state is the most stable. As the energy gap widens, fewer electrons are transferred, which results in a greater demand for energy (Ali and Abbas, 2022). The energy gap values for all computationally calculated novel ligands are displayed in (Table 13), along with the two chemical descriptors for hardness and softness. The energy gap in Neocryptomerin is the smallest of all of the potent ligands that have high softness values that it possesses suggesting that it is more stable than the other ligands that are currently the subject of research. The energy gap ranges from 4.057 to 4.425 eV. The ligand Neocryptomerin occupied the electron density region on the left side, whereas the other ligands displayed a variety of patterns (Fig. 19).

3.11 Molecular electrostatic potential (MEP)

Atomic charges are used in computer-aided drug design to investigate drug structure and biological activity. The molecular electrostatic potential, or MEP, is a measure that provides information about the electrophilic and nucleophilic regions, as well as the most suitable charge point like reagents on organic molecules (Mutlu et al., 2015). MEP contributes to a better understanding of the biological recognition process as well as the interaction between hydrogen bonds (Khan et al., 2021). To predict the different geometries' interactions at different points, MEP maps are also constructed from the same DFT functional B3LYP/6-31G**. MEP maps provide additional information in a single calculation, such as the colour grading of positive and negative regions, which can be used to find physicochemical property relationships (Suresh et al., 2022). Maximum negative areas in red are conducive to electrophilic assaults, maximum positive areas in blue are conducive to nucleophilic attacks, and zero potential areas are represented in green (Fig. 20).

3.12 Density of state analysis (DOS)

These molecules were also subjected to a density of state (DOS) examination, and the results confirmed the information provided by the FMO results. In a similar way, the DOS shows the energies of each MO of these specially-made organic donor molecules, both when it is occupied and when it is not. So, the range of energy is very important. PyMOlyze software suite is used to make DOS graphs. DOS is another approach that can be used to present the values of HOMO and LUMO along with an energy gap that can be seen in the curve pattern (**Fig. 21**), more details can be found in the supplementary material (**Table S1**).

4. Discussion

Recent years have increased interest in natural product research (Hong et al., 2019). Understanding the complex interactions between drugs and their targets and the likely mechanisms of action is made easier by the network pharmacology method (Shao and Zhang, 2013) (Alasti et al., 2006). Additionally, the variety of new drug development from plant sources poses methodological difficulties (Ma et al., 2015), due to the newly developed lack of ADME characteristics. A thunderbolt of the current era will be the identification of possibly bioactive substances that stop the pathophysiology of ailments and diseases. Medication was discovered, and because research is expensive, drug discovery methodologies face more difficulties (Zhang et al., 2019).

Lung cancer is one of the most frequently diagnosed cancers and is the leading cause of cancer-related death worldwide (Alasti et al., 2006). Non-small-cell lung cancer (NSCLC), a heterogeneous class of tumours, represents approximately 85% of all new lung cancer diagnoses (Ma et al., 2015). Tobacco smoking remains the main risk factor for developing this disease, but radon exposure and air pollution also have a role (Zhang et al., 2019). Most patients are diagnosed with advanced-stage disease owing to inadequate screening programmes and the late onset of clinical symptoms; consequently, patients have a very poor prognosis. There is currently no particularly efficient method for identifying and treating NSCLC. The most popular diagnostic technique is image detection, which is followed by genetic diagnosis (Hong et al., 2019) (Miller and Snyder, 2012). Recent methods of treating NSCLC include immunotherapy, radiotherapy, and targeted therapy. The plant family Selaginellaceae is the genus *Selaginella*, often known as spike moss, which belongs to an important group of early vascular plants (Kang et al., 2020). More than 700 different *Selaginella* species have been identified, and they are found around the world in a variety of environments, including deserts, tropical rain forests, and hilly areas (Banks, 2009) (Shim et al., 2021). Numerous bioactive substances, such as flavonoids, (neo)lignans, phenols, and alkaloids, are present in these plants (Huang et al., 2009). Significant advancements have been made in recent years in the separation of bioactive compounds from this ancestor group of primitive vascular plants. *S. tamariscina* (P. Beauv.) is a species that has drawn a lot of interest because of its long-standing use in traditional medicine and cosmetics. The pharmacological characteristics of new compounds derived from this species have been studied.

S. tamariscina (Beauv.) is used to treat multiple ailments, worldwide. Flavonoids (such as amentoflavone, hinokiflavone, sotetsuflavone, and apogenin) and saccharides make up the majority of its ingredients (e.g. trehalose, d-glucose, d-fructose and d-rhamnose) (Cheong et al., 1998). *S. tamariscina* has been shown to have antibacterial, anti-hypertensive, and anti-hyperglycemic properties in earlier research (Hsin et al., 2013) (Jeong et al., 2022) (Zheng et al., 2011). Additionally, it has been demonstrated that *S. tamariscina* possesses anti-tumor properties, most likely through the expression of the p53 tumour suppressor gene and the triggering of G1 arrest in the cell cycle in some tumour cell lines (Lee et al., 1999). Yang et al. recently discovered that *S. tamariscina* extract (STE) can reduce the expression of MMPs and u-PA and prevent lung cancer cells from migrating and metastasizing (Yang et al., 2007). Using *S. tamariscina* processes for NSCLC therapy, this study lays the groundwork for the initial screening of bioactive *S. tamariscina* compounds and introduces a novel therapeutic idea. The discovery of potential bioactive substances that halt the pathophysiology of diseases and disease will be the defining feature of this era. The current study predicted multiple target genes that are found to be engaged in several cancer-related pathways. Disease development can be prevented by focusing on the genes that disrupt cancer pathways. This may entail blocking signaling pathways, restricting migration, differentiation, and proliferation, regulating genes, metabolizing carcinogens, and inducing apoptosis by interrupting the cell cycle. (Lan et al., 2019).

The present study uncovered those target genes which are involved in different pathways in cancer. The disease can be controlled by targeting those genes that are involved to disturb the cancerous pathways. According to this research, AKT1, VEGFA, EGFR, and GSK3B are directly linked with cancer pathways, so a disturbance in these genes can cause a disease like NSCLC. further, it is confirmed by molecular docking and simulation that active compounds and key targets have stable binding forces between them. (Lee et al., 2011) demonstrated that AKT1 contributes to cell survival, albeit via different mechanisms, and that the effects on cell growth and migration are predominantly regulated by AKT1. Thus, AKT1 represents a potentially important target for chemoprevention in individuals at high risk of NSCLC. After comparison of the current findings with previous studies, it is worth noting that the majority of the compounds target AKT1 which ultimately aids in refining targeted strategies for the inhibition of AKT isoforms towards the sensitization of NSCLC cells to active compounds of *S. tamariscina*. Vascular endothelial growth factor A (VEGFA) is one of the main mediators of angiogenesis in NSCLC. Recently, it has been described as an autocrine feed-forward loop in NSCLC cells in which tumor-derived VEGFA promoted the secretion of VEGFA itself, amplifying the proangiogenic signal. (Frezza et al., 2016) reported that VEGFA regulation mainly occurred at the post-transcriptional level and that NSCLC cells expressed different isoforms of VEGFA. Collectively, the author suggested that VEGFA contributes to lung cancer progression by inducing a network of angiogenic factors, which might offer the potential for therapeutic intervention. Further, the findings of the current study also proposed that active compounds of *S. tamariscina* target VEGFA proteins which in turn assist in inhibiting the progression and proliferation of NSCLC.

EGFR is a transmembrane receptor tyrosine kinase protein that is expressed in some normal epithelial, mesenchymal, and neurogenic tissue. Recent studies (Veale et al., 1987) (Kumari et al., 2019) uncovered mutation frequency in squamous cell carcinoma. Similarly, O'Flaherty et al. reported that Glycogen synthase kinase-3 (GSK3) is over-expressed and hyperactivated in NSCLC and plays a role in ensuring the correct alignment of chromosomes on the metaphase plate during mitosis through regulation of microtubule stability. To sum up, the current study proposed multiple therapeutic targets and targeted these proteins with *S. tamariscina*-related active constituents which ultimately produce a fruitful outcome in controlling the pathogenesis of disease worldwide.

Inflammation predisposes to the development of cancer and promotes all stages of tumorigenesis. Recently, (Shim et al., 2018) reported that hinokiflavone of *S. tamariscina* has strong anti-inflammatory activities. Inflammatory responses become chronic in cancer which can result in cell mutation and proliferation and create an environment that is conducive to the development of cancer. Similarly, Apigenin has been demonstrated to show broad anti-cancer effects in various types of cancers, including colorectal cancer, breast cancer, liver cancer, lung cancer, melanoma, prostate cancer, and osteosarcoma (Xu et al., 2016) (Huang et al., 2016) (Lee et al., 2016) (Zhao et al., 2017) (Gupta et al., 2002) (Kumar et al., 2021). This flavone inhibits cancer cell proliferation by triggering cell apoptosis, inducing autophagy, and modulating the cell cycle. Apigenin also decreases cancer cell motility and inhibits cancer cell migration and invasion. Recently, apigenin was reported to show anti-cancer activities by stimulating an immune response (Cardenas et al., 2016). During those processes, multiple signaling pathways and protein kinases are modulated by apigenin, including PI3K/AKT, MAPK/ERK, JAK/STAT, NF- κ B, and Wnt/ β -catenin. Thus, targeting proteins with Heveaflavone, Neocryptomerin, Isocryptomerin, Apigenin, Sotetsuflavone, and Cryptomerin can result in reducing the chance of NSCLC in affected individuals.

GO enrichment analysis was used to discover the biological details of the target genes which revealed that target genes were mainly involved in protein phosphorylation, peptidyl-threonine phosphorylation, phosphatidylinositol 3-kinase complex, and protein serine/threonine/tyrosine kinase activity. Targets were engaged in pathways connected to liver cancer, according to KEGG pathway research. According to the KEGG pathway enrichment data, the potential targets were strongly enriched in cancer-related pathways, including the pathways for relaxin signaling, PI3K-Akt signaling, HIF-1 signaling, EGFR tyrosine inhibitor resistance, Ras signaling, and cell cycle signaling.

The compound-genes-pathway network's topological properties identified four key targets as the core targets: AKT1, VEGFA, EGFR, and GSK3B. Furthermore, these core targets were validated using molecular docking, which revealed that the phytochemicals Hinokiflavone, Heveaflavone, Neocryptomerin, Isocryptomerin, Apigenin, Sotetsuflavone, and Cryptomerin B bound stably with these core targets. These four compounds can be employed to treat NSCLC because of their capacity to bind stably with key targets, according to the results of docking studies. In light of current network pharmacology, this study predicted the active compounds, their probable targets, and associated pathways for the treatment of lung cancer, providing a theoretical foundation for subsequent experimental research. Due to network pharmacology's limitations, data mining is the sole method that can be used to identify the fundamental pharmacological mechanism for treating liver cancer. A variety of databases are particularly used in the mining of active chemicals. Despite the fact that databases are curated, there may still be a great deal of inconsistencies because of the range of information sources and experimental data. This difficulty can be resolved using contemporary high-throughput chromatographic techniques, such as liquid chromatography and mass spectrometry. Despite the compelling evidence that has been provided, more studies and clinical trials are necessary to thoroughly explore the potential of *S. tamariscina* and to confirm its potential for use in medicine.

5. Conclusions

The scientific basis for evaluating the effectiveness of multicomponent, multitarget pharmacological therapies and identifying new therapeutic targets for the treatment of NSCLC in the current research. The fundamental mechanism for the therapy of NSCLC was investigated in this study using network pharmacology and molecular docking. Network Pharmacology research reveals that *S. tamariscina* contains multi-targeting substances that work on a variety of disease-related pathways; as a result, they may be thought of as innovative therapeutic alternatives for treating NSCLC. The present research also showed that the AKT1, VEGFA, EGFR, and GSK3B genes are efficient and promising therapeutic agents for reducing NSCLC incidence and potentially showing therapeutic benefits on NSCLC. Each phytochemical reactive property was validated by exploiting the energy gap between two orbitals. Using density functional theory (DFT), the Neocryptomerin phytochemical with the lowest energy gap (4.057 eV) among the seven was revealed to be the most effective ligand for the treatment of NSCLC. Furthermore, wet lab/experimental techniques are required to validate the mechanism. Moreover, this research also provides information about the involvement of AKT1, VEGFA, EGFR, and GSK3B genes their involvement in the development of NSCLC. But further experimental techniques are required to understand the mechanism of these genes in response to liver cancer.

Author contributions

Sunil Kumar: Investigation, writing-original draft, designed and conceived the study. **Faheem Abbas:** Density-functional theory analysis. **Iqra Ali:** MD simulations and MM-GBSA analysis. **Saroj Kumar:** review & editing. **Manoj K. Gupta** and **Manoj Garg:** Conceptualization. **Deepak Kumar:** Supervision and project administration. All data were generated in-house, and no paper mill was used. All authors have read and agreed to the published version of the manuscript.

Declaration of Competing Interest

The authors confirm that there are no known conflicts of interest associated with this publication and no significant financial support for this work that could have influenced its outcome.

Acknowledgments

The authors express their gratitude to the Department of Pharmaceutical Chemistry, School of Pharmaceutical Sciences, Shoolini University, Solan, Himachal Pradesh-173229, India for the support.

Supplementary materials

Supplementary material associated with this article is submitted

References

- Agrawal, N., Mujwar, S., Goyal, A., Gupta, J.K., 2022. Phytoestrogens as Potential Antiandrogenic Agents Against Prostate Cancer: An In Silico Analysis. *Lett Drug Des Discov* 19, 69–78. <https://doi.org/10.2174/1570180818666210813121431>
- Ahmed, S.S.S.J., Ramakrishnan, V., 2012. Systems biological approach of molecular descriptors connectivity: optimal descriptors for oral bioavailability prediction. *PLoS One* 7, e40654. <https://doi.org/10.1371/journal.pone.0040654>
- Alasti, H., Cho, Y.B., Vandermeer, A.D., Abbas, A., Norrlinger, B., Shubbar, S., Bezjak, A., 2006. A novel four-dimensional radiotherapy method for lung cancer: imaging, treatment planning and delivery. *Phys Med Biol* 51, 3251. <https://doi.org/10.1088/0031-9155/51/12/017>
- Ali, U., Abbas, F., 2022. An extension of electron acceptor sites around Thiazolothiazole unit for evaluation of large power conversion efficiency: A theoretical insight. *Spectrochim Acta A Mol Biomol Spectrosc* 281, 121610. <https://doi.org/10.1016/j.saa.2022.121610>
- Aregui, A., Pluvy, J., Sanchez, M., Israel, T., Esnault, H., Guyard, A., Meyer, M., Khalil, A., Zalcman, G., Raynaud Simon, A., 2022. Measuring Walking Speed Failed to Predict Early Death and Toxicity in Elderly Patients with Metastatic Non-Small-Cell Lung Cancer (NSCLC) Selected for Undergoing First-Line Systemic

Treatment: An Observational Exploratory Study. *Cancers (Basel)* 14, 1344. <https://doi.org/10.3390/cancers14051344>

Balasundaram, A., Varghese, R.P., Siva, R., Gnanasambandan, R., Younes, S., Zayed, H., 2022. Whole-exome sequencing analysis of NSCLC reveals the pathogenic missense variants from cancer-associated genes. *Comput Biol Med* 105701. <https://doi.org/10.1016/j.compbimed.2022.105701>

Banks, J.A., 2009. Selaginella and 400 million years of separation. *Annu Rev Plant Biol* 60, 223–238. <https://doi.org/10.1146/annurev.arplant.59.032607.092851>

Batool, S., Javed, M.R., Aslam, S., Noor, F., Javed, H.M.F., Seemab, R., Rehman, A., Aslam, M.F., Paray, B.A., Gulnaz, A., 2022. Network Pharmacology and Bioinformatics Approach Reveals the Multi-Target Pharmacological Mechanism of *Fumaria indica* in the Treatment of Liver Cancer. *Pharmaceuticals* 15, 654. <https://doi.org/10.3390/ph15060654>

Blessy, J.J., Sharmila, D.J.S., 2015. Molecular simulation of N-acetylneuraminic acid analogs and molecular dynamics studies of cholera toxin-Neu5Gc complex. *J Biomol Struct Dyn* 33, 1126–1139. <https://doi.org/10.1080/07391102.2014.931825>

Boutet, E., Lieberherr, D., Tognolli, M., Schneider, M., Bairoch, A., 2007. Uniprotkb/swiss-prot, in: *Plant Bioinformatics*. Springer, pp. 89–112. https://doi.org/10.1007/978-1-59745-535-0_4

Burzić, A., Morgan, H., Baldwin, D., 2022. Epidemiology of Lung Cancer and Risk Factors. *Lung Cancer Screening* 1–11. https://doi.org/10.1007/978-3-031-10662-0_1

Cao, X., Wu, W., Wang, D., Sun, W., Lai, S., 2022. Glycogen synthase kinase GSK3 α promotes tumorigenesis by activating HIF1/VEGFA signaling pathway in NSCLC tumor. *Cell Communication and Signaling* 20, 1–16. <https://doi.org/10.1186/s12964-022-00825-3>

Cardenas, H., Arango, D., Nicholas, C., Duarte, S., Nuovo, G.J., He, W., Voss, O.H., Gonzalez-Mejia, M.E., Guttridge, D.C., Grotewold, E., 2016. Dietary apigenin exerts immune-regulatory activity in vivo by reducing NF- κ B activity, halting leukocyte infiltration and restoring normal metabolic function. *Int J Mol Sci* 17, 323. <https://doi.org/10.3390/ijms17030323>

Chaft, J.E., Shyr, Y., Sepesi, B., Forde, P.M., 2022. Preoperative and postoperative systemic therapy for operable non-small-cell lung cancer. *Journal of Clinical Oncology* 40, 546–555. <https://doi.org/10.1200/JCO.21.01589>

Chandran, K., Shane, D.I., Zochedh, A., Sultan, A.B., Kathiresan, T., 2022. Docking simulation and ADMET prediction based investigation on the phytochemical constituents of Noni (*Morinda citrifolia*) fruit as a potential anticancer drug. *In Silico Pharmacol* 10, 1–14. <https://doi.org/10.1007/s40203-022-00130-4>

- CHEBAIBI, M., Bousta, D., Gonçalves, R.F.B., Hoummani, H., Achour, S., 2021. Medicinal Plants Against Coronavirus (SARS-COV-2) in Morocco Via Computational Virtual Screening Approach. <https://doi.org/10.21203/rs.3.rs-679827/v1>
- Chen, P., Solomon, E.I., 2002. Frontier molecular orbital analysis of Cun–O₂ reactivity. *J Inorg Biochem* 88, 368–374. [https://doi.org/10.1016/S0162-0134\(01\)00349-X](https://doi.org/10.1016/S0162-0134(01)00349-X)
- Cheong, H., Ryu, S.-Y., Oak, M.-H., Cheon, S.-H., Yoo, G.-S., Kim, K.-M., 1998. Studies of structure activity relationship of flavonoids for the anti-allergic actions. *Arch Pharm Res* 21, 478–480. <https://doi.org/10.1007/BF02974647>
- Civalleri, B., Zicovich-Wilson, C.M., Valenzano, L., Ugliengo, P., 2008. B3LYP augmented with an empirical dispersion term (B3LYP-D*) as applied to molecular crystals. *CrystEngComm* 10, 405–410. <https://doi.org/10.1039/B715018K>
- Cooper, Z.D., 2016. Adverse effects of synthetic cannabinoids: management of acute toxicity and withdrawal. *Curr Psychiatry Rep* 18, 1–10. <https://doi.org/10.1007/s11920-016-0694-1>
- Daina, A., Michielin, O., Zoete, V., 2017. SwissADME: a free web tool to evaluate pharmacokinetics, drug-likeness and medicinal chemistry friendliness of small molecules. *Sci Rep* 7, 1–13. <https://doi.org/10.1038/srep42717>
- Dhameliya, T.M., Nagar, P.R., Gajjar, N.D., 2022. Systematic virtual screening in search of SARS CoV-2 inhibitors against spike glycoprotein: pharmacophore screening, molecular docking, ADMET analysis and MD simulations. *Mol Divers* 1–18. <https://doi.org/10.1007/s11030-022-10394-9>
- Dilshad, R., Ahmad, S., Aati, H.Y., Al-qahtani, J.H., Sherif, A.E., Hussain, M., Ghalloo, B.A., Tahir, H., Basit, A., Ahmed, M., 2022. Phytochemical profiling, in vitro biological activities, and in-silico molecular docking studies of *Typha domingensis*. *Arabian Journal of Chemistry* 15, 104133. <https://doi.org/10.1016/j.arabjc.2022.104133>
- Frezzetti, D., Gallo, M., Roma, C., D'Alessio, A., Maiello, M.R., Bevilacqua, S., Normanno, N., de Luca, A., 2016. Vascular endothelial growth factor a regulates the secretion of different angiogenic factors in lung cancer cells. *J Cell Physiol* 231, 1514–1521. <https://doi.org/10.1002/jcp.25243>
- Fung, V., Hu, G., Ganesh, P., Sumpter, B.G., 2021. Machine learned features from density of states for accurate adsorption energy prediction. *Nat Commun* 12, 1–11. <https://doi.org/10.1038/s41467-020-20342-6>
- Gao, L., Yin, S., Li, Z., Sha, Y., Pei, Y., Shi, G., Jing, Y., Hua, H., 2007. Three novel sterols isolated from *Selaginella tamariscina* with antiproliferative activity in leukemia cells. *Planta Med* 73, 1112–1115. <https://doi.org/DOI:%2010.1055/s-2007-981562>

- Gfeller, D., Grosdidier, A., Wirth, M., Daina, A., Michielin, O., Zoete, V., 2014. SwissTargetPrediction: a web server for target prediction of bioactive small molecules. *Nucleic Acids Res* 42, W32–W38. <https://doi.org/10.1093/nar/gku293>
- Gupta, S., Afaq, F., Mukhtar, H., 2002. Involvement of nuclear factor-kappa B, Bax and Bcl-2 in induction of cell cycle arrest and apoptosis by apigenin in human prostate carcinoma cells. *Oncogene* 21, 3727–3738. <https://doi.org/10.1038/sj.onc.1205474>
- Haghi, A., Raissi, H., Hashemzadeh, H., Farzad, F., 2022. Development of the poly (1-histidine) grafted carbon nanotube as a possible smart drug delivery vehicle. *Comput Biol Med* 143, 105336. <https://doi.org/10.1016/j.compbiomed.2022.105336>
- He, X.-R., Xu, L.-Y., Jin, C., Yue, P.-F., Zhou, Z.-W., Liang, X.-L., 2019. Tamariscinols U–W, new dihydrobenzofuran-type norneolignans with tyrosinase inhibitory activity from *Selaginella tamariscina*. *Phytochem Lett* 34, 79–83. <https://doi.org/10.1016/j.phytol.2019.08.013>
- Hertwig, R.H., Koch, W., 1997. On the parameterization of the local correlation functional. What is Becke-3-LYP? *Chem Phys Lett* 268, 345–351. [https://doi.org/10.1016/S0009-2614\(97\)00207-8](https://doi.org/10.1016/S0009-2614(97)00207-8)
- Hong, G.-S., Do, K.-H., Lee, C.W., 2019. Added Value of Bone Suppression Image in the Detection of Subtle Lung Lesions on Chest Radiographs with Regard to Reader's Expertise. *J Korean Med Sci* 34. <https://doi.org/10.3346/jkms.2019.34.e250>
- Hsin, C.-H., Wu, B.-C., Chuang, C.-Y., Yang, S.-F., Hsieh, Y.-H., Ho, H.-Y., Lin, H.-P., Chen, M.-K., Lin, C.-W., 2013. *Selaginella tamariscina* extract suppresses TPA-induced invasion and metastasis through inhibition of MMP-9 in human nasopharyngeal carcinoma HONE-1 cells. *BMC Complement Altern Med* 13, 234. <https://doi.org/10.1186/1472-6882-13-234>
- Huang, C., Wei, Y.-X., Shen, M.-C., Tu, Y.-H., Wang, C.-C., Huang, H.-C., 2016. Chrysin, abundant in *Morinda citrifolia* fruit water–etoac extracts, combined with apigenin synergistically induced apoptosis and inhibited migration in human breast and liver cancer cells. *J Agric Food Chem* 64, 4235–4245. <https://doi.org/10.1021/acs.jafc.6b00766>
- Huang, D.W., Sherman, B.T., Tan, Q., Collins, J.R., Alvord, W.G., Roayaei, J., Stephens, R., Baseler, M.W., Lane, H.C., Lempicki, R.A., 2007. The DAVID Gene Functional Classification Tool: a novel biological module-centric algorithm to functionally analyze large gene lists. *Genome Biol* 8, 1–16. <https://doi.org/10.1186/gb-2007-8-9-r183>
- Huang, W.-Y., Cai, Y.-Z., Zhang, Y., 2009. Natural phenolic compounds from medicinal herbs and dietary plants: potential use for cancer prevention. *Nutr Cancer* 62, 1–20. <https://doi.org/10.1080/01635580903191585>

Huber, R.M., Cavic, M., Kerpel-Fronius, A., Viola, L., Field, J., Jiang, L., Kazerooni, E.A., Koegelenberg, C.F.N., Mohan, A., Dos Santos, R.S., 2022. Lung cancer screening considerations during respiratory infection outbreaks, epidemics or pandemics: an international association for the study of lung cancer early detection and screening committee report. *Journal of Thoracic Oncology* 17, 228–238.

<https://doi.org/10.1016/j.jtho.2021.11.008>

Ibrahim, O.H.M., Abo-Elyousr, K.A.M., Asiry, K.A., Alhakamy, N.A., Mousa, M.A.A., 2022. Phytochemical characterization, antimicrobial activity and in vitro antiproliferative potential of *Alchemilla vulgaris* Auct root extract against prostate (PC-3), breast (MCF-7) and colorectal adenocarcinoma (Caco-2) cancer cell lines. *Plants* 11, 2140.

<https://doi.org/10.3390/plants11162140>

James, T., Hsieh, M.-L., Knipling, L., Hinton, D., 2015. Determining the Architecture of a Protein–DNA Complex by Combining FeBABE Cleavage Analyses, 3-D Printed Structures, and the ICM Molsoft Program, in: *DNA-Protein Interactions*. Springer, pp. 29–40.

https://doi.org/10.1007/978-1-4939-2877-4_3

Jeong, Y.H., Kim, T.I., Oh, Y.-C., Ma, J.Y., 2022. *Selaginella tamariscina* Inhibits Glutamate-Induced Autophagic Cell Death by Activating the PI3K/AKT/mTOR Signaling Pathways. *Int J Mol Sci* 23, 11445.

<https://doi.org/10.3390/ijms231911445>

Jumbo, L.O.V., Corrêa, M.J.M., Gomes, J.M., Armijos, M.J.G., Valarezo, E., Mantilla-Afanador, J.G., Machado, F.P., Rocha, L., Aguiar, R.W.S., Oliveira, E.E., 2022. Potential of *Bursera graveolens* essential oil for controlling bean weevil infestations: Toxicity, repellence, and action targets. *Ind Crops Prod* 178, 114611.

<https://doi.org/10.1016/j.indcrop.2022.114611>

Kang, J., Zhang, H., Wang, Y., Liang, S., Mao, Z., Zhang, X., Xiang, Q., 2020. Distinctive evolutionary pattern of organelle genomes linked to the nuclear genome in Selaginellaceae. *The Plant Journal* 104, 1657–1672.

<https://doi.org/10.1111/tbj.15028>

Kennedy, K., Hulbert, A., Pasquinelli, M., Feldman, L.E., 2022. Impact of CT screening in lung cancer: Scientific evidence and literature review, in: *Seminars in Oncology*. Elsevier.

<https://doi.org/10.1053/j.seminoncol.2022.06.013>

Khan, J., Sakib, S.A., Mahmud, S., Khan, Z., Islam, M.N., Sakib, M.A., Emran, T. Bin, Simal-Gandara, J., 2021. Identification of potential phytochemicals from Citrus limon against main protease of SARS-CoV-2: Molecular docking, molecular dynamic simulations and quantum computations. *J Biomol Struct Dyn* 1–12.

<https://doi.org/10.1080/07391102.2021.1947893>

Kim, S., Thiessen, P.A., Bolton, E.E., Chen, J., Fu, G., Gindulyte, A., Han, L., He, J., He, S., Shoemaker, B.A., 2016a. PubChem substance and compound databases. *Nucleic Acids Res* 44, D1202–D1213.

<https://doi.org/10.1016/j.jmb.2022.167514>

- Kim, S., Thiessen, P.A., Bolton, E.E., Chen, J., Fu, G., Gindulyte, A., Han, L., He, J., He, S., Shoemaker, B.A., 2016b. PubChem substance and compound databases. *Nucleic Acids Res* 44, D1202–D1213. <https://doi.org/10.1016/j.jmb.2022.167514>
- Klepeis, J.L., Lindorff-Larsen, K., Dror, R.O., Shaw, D.E., 2009. Long-timescale molecular dynamics simulations of protein structure and function. *Curr Opin Struct Biol* 19, 120–127. <https://doi.org/10.1016/j.sbi.2009.03.004>
- Kouranov, A., Xie, L., de la Cruz, J., Chen, L., Westbrook, J., Bourne, P.E., Berman, H.M., 2006. The RCSB PDB information portal for structural genomics. *Nucleic Acids Res* 34, D302–D305. <https://doi.org/10.1093/nar/gkj120>
- Kumar, S., Sharma, A.K., Lalhlenmawia, H., Kumar, D., 2021. Natural Compounds Targeting Major Signaling Pathways in Lung Cancer. *Targeting Cellular Signalling Pathways in Lung Diseases* 821–846. https://doi.org/10.1007/978-981-33-6827-9_37
- Kumari, N., Singh, S., Haloi, D., Mishra, S.K., Krishnani, N., Nath, A., Neyaz, Z., 2019. Epidermal growth factor receptor mutation frequency in squamous cell carcinoma and its diagnostic performance in cytological samples: a molecular and immunohistochemical study. *World J Oncol* 10, 142. <https://doi.org/10.14740%2Fwjon1204>
- Lan, L., Wang, Y., Pan, Z., Wang, B., Yue, Z., Jiang, Z., Li, L., Wang, C., Tang, H., 2019. Rhamnetin induces apoptosis in human breast cancer cells via the miR 34a/Notch 1 signaling pathway. *Oncol Lett* 17, 676–682. <https://doi.org/10.3892/ol.2018.9575>
- Lee, I.-S., Nishikawa, A., Furukawa, F., Kasahara, K., Kim, S.-U., 1999. Effects of *Selaginella tamariscina* on in vitro tumor cell growth, p53 expression, G1 arrest and in vivo gastric cell proliferation. *Cancer Lett* 144, 93–99. [https://doi.org/10.1016/S0304-3835\(99\)00202-5](https://doi.org/10.1016/S0304-3835(99)00202-5)
- Lee, M.W., Kim, D.S., Lee, J.H., Lee, B.S., Lee, S.H., Jung, H.L., Sung, K.W., Kim, H.T., Yoo, K.H., Koo, H.H., 2011. Roles of AKT1 and AKT2 in non-small cell lung cancer cell survival, growth, and migration. *Cancer Sci* 102, 1822–1828. <https://doi.org/10.1111/j.1349-7006.2011.02025.x>
- Lee, Y.-M., Lee, G., Oh, T.-I., Kim, B.M., Shim, D.-W., Lee, K.-H., Kim, Y.J., Lim, B.O., Lim, J.-H., 2016. Inhibition of glutamine utilization sensitizes lung cancer cells to apigenin-induced apoptosis resulting from metabolic and oxidative stress. *Int J Oncol* 48, 399–408. <https://doi.org/10.3892/ijo.2015.3243>
- Lei, Yu, Lei, Yan, Shi, X., Wang, J., 2022. EML4 ALK fusion gene in non small cell lung cancer. *Oncol Lett* 24, 1–6. <https://doi.org/10.3892/ol.2022.13397>
- Li, A.P., 2001. Screening for human ADME/Tox drug properties in drug discovery. *Drug Discov Today* 6, 357–366. [https://doi.org/10.1016/S1359-6446\(01\)01712-3](https://doi.org/10.1016/S1359-6446(01)01712-3)

- Lin, L.-C., Kuo, Y.-C., Chou, C.-J., 2000. Cytotoxic biflavonoids from *Selaginella delicatula*. *J Nat Prod* 63, 627–630. <https://doi.org/10.1021/np990538m>
- Ma, Z.-L., Zhang, B.-J., Wang, D.-T., Li, X., Wei, J.-L., Zhao, B.-T., Jin, Y., Li, Y.-L., Jin, Y.-X., 2015. Tanshinones suppress AURKA through up-regulation of miR-32 expression in non-small cell lung cancer. *Oncotarget* 6, 20111. <https://doi.org/10.18632/oncotarget.3933>
- Madeddu, C., Donisi, C., Liscia, N., Lai, E., Scartozzi, M., Macciò, A., 2022. Egfr-mutated non-small cell lung cancer and resistance to immunotherapy: Role of the tumor microenvironment. *Int J Mol Sci* 23, 6489. <https://doi.org/10.3390/ijms23126489>
- Madhavi Sastry, G., Adzhigirey, M., Day, T., Annabhimoju, R., Sherman, W., 2013. Protein and ligand preparation: Parameters, protocols, and influence on virtual screening enrichments. *J Comput Aided Mol Des* 27, 221–234. <https://doi.org/10.1007/s10822-013-9644-8>
- Mering, C. von, Huynen, M., Jaeggi, D., Schmidt, S., Bork, P., Snel, B., 2003. STRING: a database of predicted functional associations between proteins. *Nucleic Acids Res* 31, 258–261. <https://doi.org/10.1093/nar/gkg034>
- Miller, P.E., Snyder, D.C., 2012. Phytochemicals and cancer risk: a review of the epidemiological evidence. *Nutrition in Clinical Practice* 27, 599–612. <https://doi.org/10.1177/0884533612456043>
- Mlilo, S., Sibanda, S., 2022. An ethnobotanical survey of the medicinal plants used in the treatment of cancer in some parts of Matebeleland, Zimbabwe. *South African Journal of Botany* 146, 401–408. <https://doi.org/10.1016/j.sajb.2021.11.022>
- Mohanraj, K., Karthikeyan, B.S., Vivek-Ananth, R.P., Chand, R.P., Aparna, S.R., Mangalapandi, P., Samal, A., 2018. IMPPAT: a curated database of Indian medicinal plants, phytochemistry and therapeutics. *Sci Rep* 8, 1–17. <https://doi.org/10.1038/s41598-018-22631-z>
- Motallebi, M., Bhia, M., Rajani, H.F., Bhia, I., Tabarraei, H., Mohammadkhani, N., Pereira-Silva, M., Kasaii, M.S., Nouri-Majd, S., Mueller, A.-L., 2022. Naringenin: A potential flavonoid phytochemical for cancer therapy. *Life Sci* 120752. <https://doi.org/10.1016/j.lfs.2022.120752>
- Mutlu, O., Akar, F., Celikyurt, I.K., Tanyeri, P., Ulak, G., Erden, F., 2015. 7-NI and ODQ disturbs memory in the elevated plus maze, Morris water maze, and radial arm maze tests in mice. *Drug Target Insights* 9, DTI-S23378. <https://doi.org/10.4137/DTI.S23378>
- Naeem, I., Mateen, R.M., Sibtul Hassan, S., Tariq, A., Parveen, R., Saqib, M.A.N., Fareed, M.I., Hussain, M., Afzal, M.S., 2022. In silico identification of potential drug-like molecules against G glycoprotein of Nipah virus by molecular docking, DFT studies, and molecular dynamic simulation. *J Biomol Struct Dyn* 1–15. <https://doi.org/10.1080/07391102.2022.2115557>

- Nguyen, P.T.V., Huynh, H.A., Truong, D. Van, Tran, T.-D., Vo, C.-V.T., 2020. Exploring aurone derivatives as potential human pancreatic lipase inhibitors through molecular docking and molecular dynamics simulations. *Molecules* 25, 4657. <https://doi.org/10.3390/molecules25204657>
- Noor, F., Rehman, A., Ashfaq, U.A., Saleem, M.H., Okla, M.K., Al-Hashimi, A., AbdElgawad, H., Aslam, S., 2022a. Integrating Network Pharmacology and Molecular Docking Approaches to Decipher the Multi-Target Pharmacological Mechanism of *Abrus precatorius* L. Acting on Diabetes. *Pharmaceuticals* 15, 414. <https://doi.org/10.3390/ph15040414>
- Noor, F., Tahir ul Qamar, M., Ashfaq, U.A., Albutti, A., Alwashmi, A.S.S., Aljasir, M.A., 2022b. Network Pharmacology Approach for Medicinal Plants: Review and Assessment. *Pharmaceuticals* 15, 572. <https://doi.org/10.3390/ph15050572>
- Obot, I.B., Macdonald, D.D., Gasem, Z.M., 2015. Density functional theory (DFT) as a powerful tool for designing new organic corrosion inhibitors. Part 1: an overview. *Corros Sci* 99, 1–30. <https://doi.org/10.1016/j.corsci.2015.01.037>
- Oyedele, A.-Q.K., Ogunlana, A.T., Boyenle, I.D., Adeyemi, A.O., Rita, T.O., Adelusi, T.I., Abdul-Hammed, M., Elegbeleye, O.E., Odunitan, T.T., 2022. Docking covalent targets for drug discovery: stimulating the computer-aided drug design community of possible pitfalls and erroneous practices. *Mol Divers* 1–25. <https://doi.org/10.1007/s11030-022-10523-4>
- Pan, X., Dvortsin, E., Aerts, J., Baldwin, D.R., Groen, H.J.M., Ramaker, D., Velikanova, R., Oudkerk, M., Postma, M.J., 2022. P1. 02-03 Budget Impact Analysis of Volume CT Lung Cancer Screening Based on NELSON Study Outcomes in Europe. *Journal of Thoracic Oncology* 17, S99. <https://doi.org/10.1016/j.jtho.2022.07.164>
- Pattar, S.V., Adhoni, S.A., Kamanavalli, C.M., Kumbar, S.S., 2020. In silico molecular docking studies and MM/GBSA analysis of coumarin-carbonodithioate hybrid derivatives divulge the anticancer potential against breast cancer. *Beni Suef Univ J Basic Appl Sci* 9, 1–10. <https://doi.org/10.1186/s43088-020-00059-7>
- Pence, H.E., Williams, A., 2010. ChemSpider: an online chemical information resource. <https://doi.org/10.1021/ed100697w>
- Rasheed, M.A., Iqbal, M.N., Saddick, S., Ali, I., Khan, F.S., Kanwal, S., Ahmed, D., Ibrahim, M., Afzal, U., Awais, M., 2021. Identification of lead compounds against scm (Fms10) in enterococcus faecium using computer aided drug designing. *Life* 11. <https://doi.org/10.3390/life11020077>
- Rekowska, A., Rola, P., Wójcik-Superczyńska, M., Chmielewska, I., Krawczyk, P., Milanowski, J., 2022. Efficacy of Osimertinib in Lung Squamous Cell Carcinoma Patients with EGFR Gene Mutation—Case Report and A Literature Review. *Current Oncology* 29, 3531–3539. <https://doi.org/10.3390/curroncol29050285>

- Safran, M., Dalah, I., Alexander, J., Rosen, N., Iny Stein, T., Shmoish, M., Nativ, N., Bahir, I., Doniger, T., Krug, H., 2010. GeneCards Version 3: the human gene integrator. Database 2010. <https://doi.org/10.1093/database/baq020>
- Saravanan, S., Balachandran, V., 2014. Quantum chemical studies, natural bond orbital analysis and thermodynamic function of 2, 5-dichlorophenylisocyanate. Spectrochim Acta A Mol Biomol Spectrosc 120, 351–364. <https://doi.org/10.1016/j.saa.2013.10.042>
- Selick, H.E., Beresford, A.P., Tarbit, M.H., 2002. The emerging importance of predictive ADME simulation in drug discovery. Drug Discov Today 7, 109–116. [https://doi.org/10.1016/S1359-6446\(01\)02100-6](https://doi.org/10.1016/S1359-6446(01)02100-6)
- Shakil, S., 2021. Molecular interaction of inhibitors with human brain butyrylcholinesterase. EXCLI J 20, 1597. <https://doi.org/10.17179/excli2021-4418>
- Shao, L.I., Zhang, B., 2013. Traditional Chinese medicine network pharmacology: theory, methodology and application. Chin J Nat Med 11, 110–120. [https://doi.org/10.1016/S1875-5364\(13\)60037-0](https://doi.org/10.1016/S1875-5364(13)60037-0)
- Shim, H., Lee, H.J., Lee, J., Lee, H.-O., Kim, J.-H., Yang, T.-J., Kim, N.-S., 2021. Plastid genomes of the early vascular plant genus Selaginella have unusual direct repeat structures and drastically reduced gene numbers. Int J Mol Sci 22, 641. <https://doi.org/10.3390/ijms22020641>
- Shim, S.-Y., Lee, S., Lee, M., 2018. Biflavonoids isolated from Selaginella tamariscina and their anti-inflammatory activities via ERK 1/2 signaling. Molecules 23, 926. <https://doi.org/10.3390/molecules23040926>
- Shinbo, Y., Nakamura, Y., Altaf-Ul-Amin, M., Asahi, H., Kurokawa, K., Arita, M., Saito, K., Ohta, D., Shibata, D., Kanaya, S., 2006. KNApSACk: a comprehensive species-metabolite relationship database, in: Plant Metabolomics. Springer, pp. 165–181. https://doi.org/10.1007/3-540-29782-0_13
- Shivakumar, D., Williams, J., Wu, Y., Damm, W., Shelley, J., Sherman, W., 2010. Prediction of absolute solvation free energies using molecular dynamics free energy perturbation and the oplis force field. J Chem Theory Comput 6, 1509–1519. <https://doi.org/10.1021/ct900587b>
- Smoot, M.E., Ono, K., Ruscheinski, J., Wang, P.-L., Ideker, T., 2011. Cytoscape 2.8: new features for data integration and network visualization. Bioinformatics 27, 431–432. <https://doi.org/10.1093/bioinformatics/btq675>
- Suresh, C.H., Remya, G.S., Anjalikrishna, P.K., 2022. Molecular electrostatic potential analysis: A powerful tool to interpret and predict chemical reactivity. Wiley Interdiscip Rev Comput Mol Sci e1601. <https://doi.org/10.1002/wcms.1601>

- Syarafina, Z.Y.I., Safithri, M., Bintang, M., Kurniasih, R., 2022. In Silico Screening of Cinnamon (*Cinnamomum burmannii*) Bioactive Compounds as Acetylcholinesterase Inhibitors. *Jurnal Kimia Sains dan Aplikasi* 25, 97–107. <https://doi.org/10.14710/jksa.25.3.97-107>
- Szklarczyk, D., Santos, A., Von Mering, C., Jensen, L.J., Bork, P., Kuhn, M., 2016. STITCH 5: augmenting protein–chemical interaction networks with tissue and affinity data. *Nucleic Acids Res* 44, D380–D384. <https://doi.org/10.1093/nar/gkv1277>
- Tanveer, F., Anwar, M.F., Siraj, B., Zarina, S., 2021. Evaluation of anti-EGFR potential of quinazoline derivatives using molecular docking: An in silico approach. *Biotechnol Appl Biochem.* <https://doi.org/10.1002/bab.2199>
- Tromer, R.M., Felix, L.C., Woellner, C.F., Galvao, D.S., 2021. A DFT investigation of the electronic, optical, and thermoelectric properties of pentadiamond. *Chem Phys Lett* 763, 138210. <https://doi.org/10.1016/j.cplett.2020.138210>
- Tuorkey, M.J., 2015. Cancer Therapy with Phytochemicals: Present and Future Perspectives. *Biomedical and Environmental Sciences* 28, 808–819. [https://doi.org/10.1016/S0895-3988\(15\)30111-2](https://doi.org/10.1016/S0895-3988(15)30111-2)
- Veale, D., Ashcroft, T., Marsh, C., Gibson, G.J., Harris, A.L., 1987. Epidermal growth factor receptors in non-small cell lung cancer. *Br J Cancer* 55, 513–516. <https://doi.org/10.1038/bjc.1987.104>
- Wang, Y., Zhang, H., Liu, C., Wang, Z., Wu, W., Zhang, N., Zhang, L., Hu, J., Luo, P., Zhang, J., 2022. Immune checkpoint modulators in cancer immunotherapy: Recent advances and emerging concepts. *J Hematol Oncol* 15, 1–53. <https://doi.org/10.1186/s13045-022-01325-0>
- Wen, J., Zheng, X., Liu, C., Nie, C.-D., Jiang, Y.-Y., Sun, X.-M., Li, W.-L., Yan, X.-J., 2021. Two new selariscinins from *Selaginella tamariscina* (Beauv.) Spring. *J Asian Nat Prod Res* 23, 675–680. <https://doi.org/10.1080/10286020.2020.1810672>
- Xiong, G., Wu, Z., Yi, J., Fu, L., Yang, Z., Hsieh, C., Yin, M., Zeng, X., Wu, C., Lu, A., Chen, X., Hou, T., Cao, D., 2021. ADMETlab 2.0: an integrated online platform for accurate and comprehensive predictions of ADMET properties. *Nucleic Acids Res* 49, W5–W14. <https://doi.org/10.1093/nar/gkab255>
- Xu, M., Wang, S., Song, Y.U., Yao, J., Huang, K., Zhu, X., 2016. Apigenin suppresses colorectal cancer cell proliferation, migration and invasion via inhibition of the Wnt/ β -catenin signaling pathway. *Oncol Lett* 11, 3075–3080. <https://doi.org/10.3892/ol.2016.4331>
- Xu, X., Zhang, W., Huang, C., Li, Y., Yu, H., Wang, Y., Duan, J., Ling, Y., 2012. A novel chemometric method for the prediction of human oral bioavailability. *Int J Mol Sci* 13, 6964–6982. <https://doi.org/10.3390/ijms13066964>

- Yang, S.F., Chu, S.C., Liu, S.J., Chen, Y.C., Chang, Y.Z., Hsieh, Y.S., 2007. Antimetastatic activities of *Selaginella tamariscina* (Beauv.) on lung cancer cells in vitro and in vivo. *J Ethnopharmacol* 110, 483–489. <https://doi.org/10.1016/j.jep.2006.10.010>
- Zhang, R., Zhu, Z., Lv, H., Li, F., Sun, S., Li, J., Lee, C., 2019. Immune checkpoint blockade mediated by a small-molecule nanoinhibitor targeting the PD-1/PD-L1 pathway synergizes with photodynamic therapy to elicit antitumor immunity and antimetastatic effects on breast cancer. *Small* 15, 1903881. <https://doi.org/10.1002/sml.201903881>
- Zhang, X., Perez-Sanchez, H., Lightstone, F.C., 2017. A Comprehensive Docking and MM/GBSA Rescoring Study of Ligand Recognition upon Binding Antithrombin. *Curr Top Med Chem* 17, 1631. <https://doi.org/10.2174/1568026616666161117112604>
- Zhao, G., Han, X., Cheng, W., Ni, J., Zhang, Y., Lin, J., Song, Z., 2017. Apigenin inhibits proliferation and invasion, and induces apoptosis and cell cycle arrest in human melanoma cells. *Oncol Rep* 37, 2277–2285. <https://doi.org/10.3892/or.2017.5450>
- Zheng, X., Zhang, L., Wang, W., Wu, Y., Zhang, Q., Feng, W., 2011. Anti-diabetic activity and potential mechanism of total flavonoids of *Selaginella tamariscina* (Beauv.) Spring in rats induced by high fat diet and low dose STZ. *J Ethnopharmacol* 137, 662–668. <https://doi.org/10.1016/j.jep.2011.06.018>
- Zochedh, A., Priya, M., Shunmuganarayanan, A., Thandavarayan, K., Sultan, A.B., 2022. Investigation on structural, spectroscopic, DFT, biological activity and molecular docking simulation of essential oil Gamma-Terpinene. *J Mol Struct* 1268, 133651. <https://doi.org/10.1016/j.molstruc.2022.133651>

Figure Legends

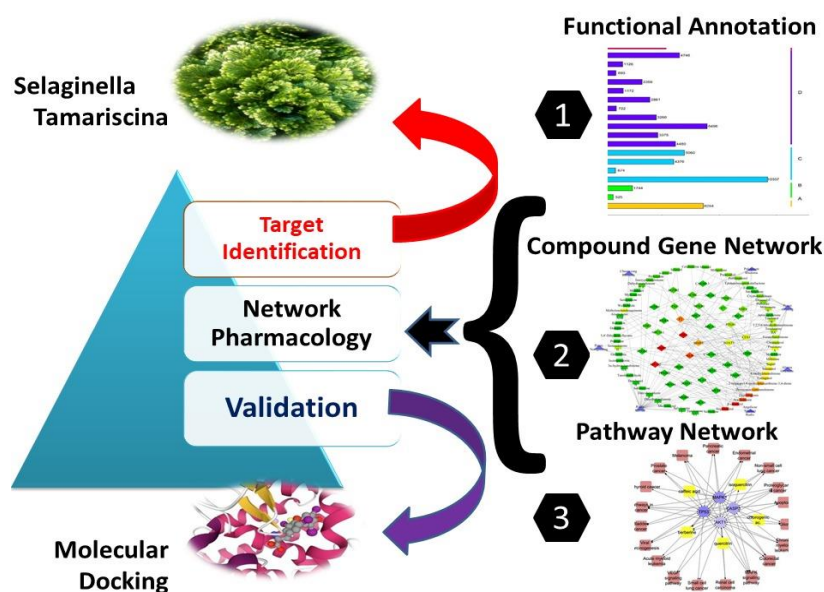


Fig. 1. A graphical summary of the overall technique used to anticipate prospective chemicals and their potential targets for lung cancer treatment.

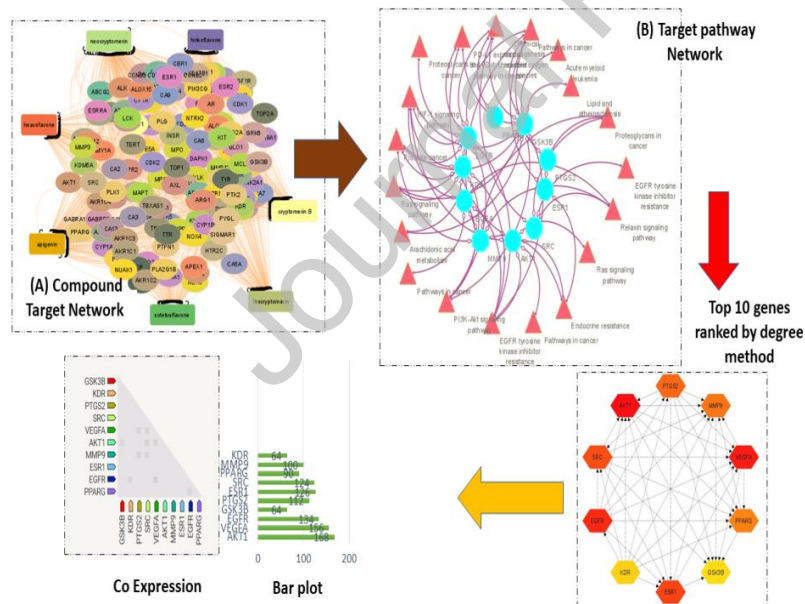


Fig. 2. Analysis of multi-compound, multi-target, and multi-pathway lung cancer treatment using network pharmacology (A) Compound network diagram with objectives. (B) Target gene enrichment pathway network diagram. (C) The top ten genes are ordered by degree (D) The PPI network Bar plot (E) Seven Target genes were expressed in Homo sapiens.

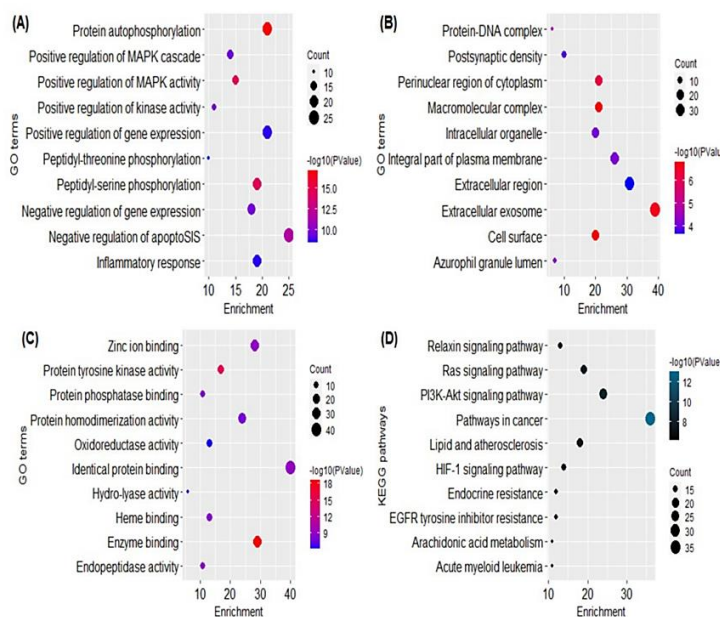


Fig. 3. Representation of functional annotation and enriched pathways in form of Bubble Plot. **(A)** GO in terms of biological processes. **(B)** GO in terms of molecular function. **(C)** GO in terms of cellular components. **(D)** KEGG pathway analysis

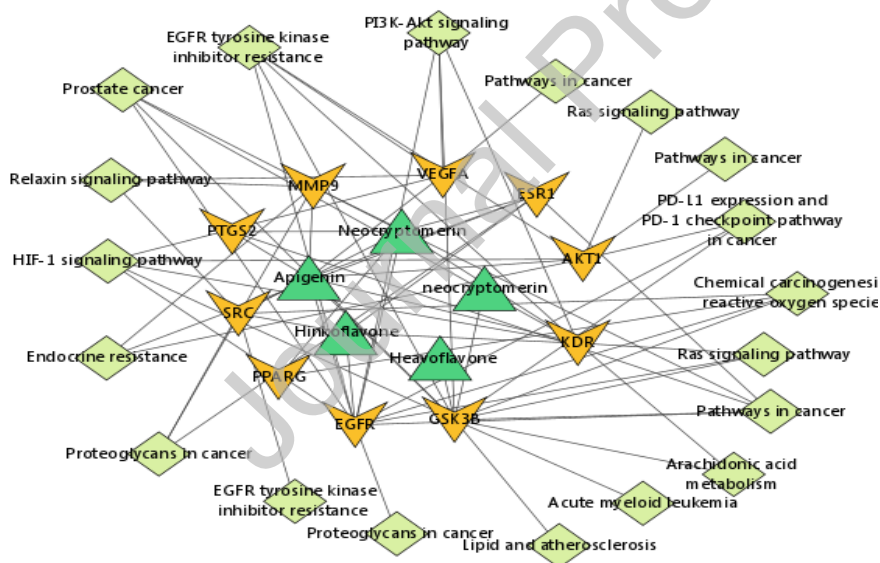


Fig. 4. The hub genes are represented by the green nodes, the yellow nodes, represent active substances, while the pathways connected to the primary targets are represented by the light green nodes.

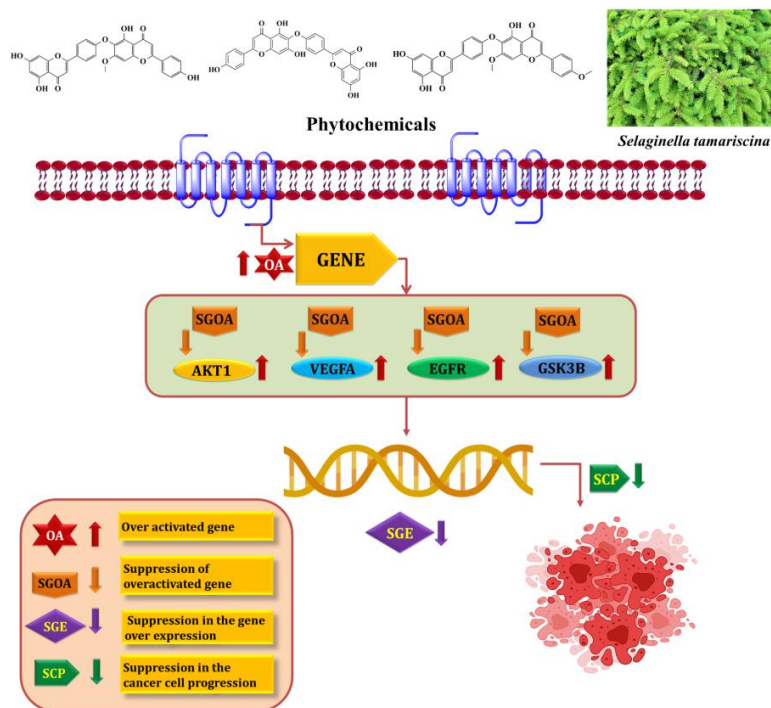


Fig. 5. The molecular mechanism of the phytochemicals from the *Selaginella tamariscina* on the targeted genes AKT1, VEGFR, EGFR, and GSK3B.

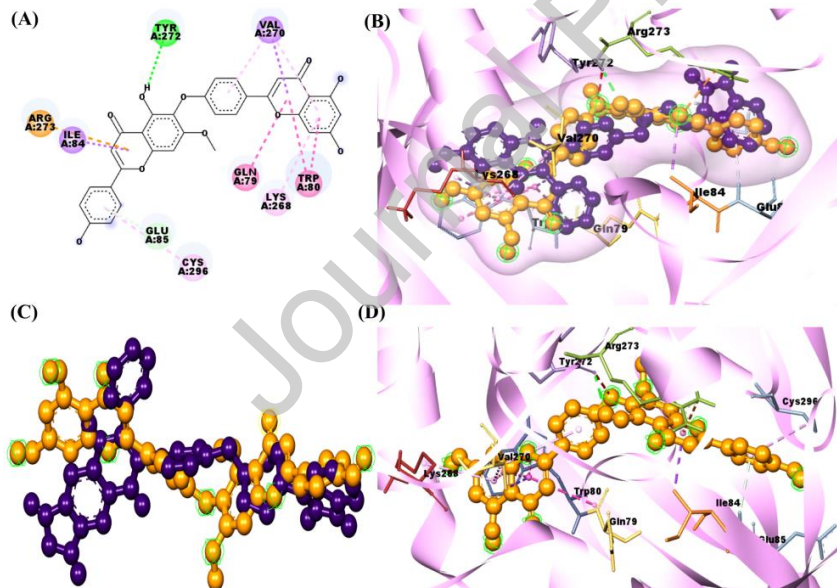


Fig. 6. (A) 2D interaction diagram showing the types of contacts formed between crystallographic receptors as anticancer target AKT1 (PDB ID: 3O96) and isocryptomerin. The green dotted lines indicate H-bonding. (B) Surface mapping of isocryptomerin having golden color inside the active site of (PDB ID: 3O96) along with reference molecule. The reference molecule indicated in the purple color. (C) Represents the superimposed docked pose of isocryptomerin with crystallographic receptors as anticancer targets AKT1. (D) Represents the

3D interaction of isocryptomerin at its active site. The protein structure is indicated in light pink color; the isocryptomerin is indicated in golden color; the amino acid residues are indicated in the black color.

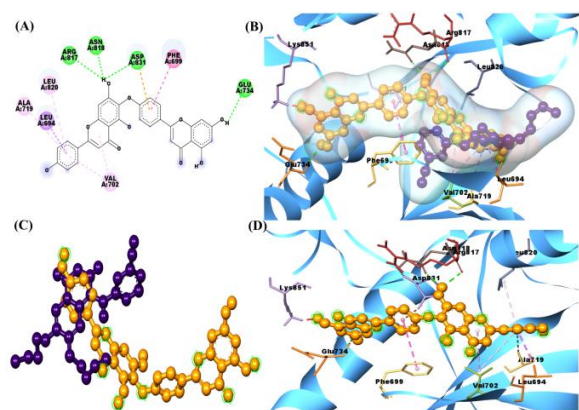


Fig. 7. (A) 2D interaction diagram showing the types of contacts formed between EGFR tyrosine kinase receptor (PDB ID: 1M17) and hinokiflavone. The green dotted lines indicate H-bonding. (B) Surface mapping of hinokiflavone having golden color inside the active site of (PDB ID: 1M17) along with reference molecule. The reference molecule is indicated in the purple color. (C) Represents the superimposed docked pose of hinokiflavone with EGFR tyrosine kinase receptor co-crystallized ligand erlotinib. (D) Represents the 3D interaction of hinokiflavone at its active site. The protein structure is indicated in light blue color; the hinokiflavone molecule is indicated in golden color; the amino acid residues are indicated in the black color.

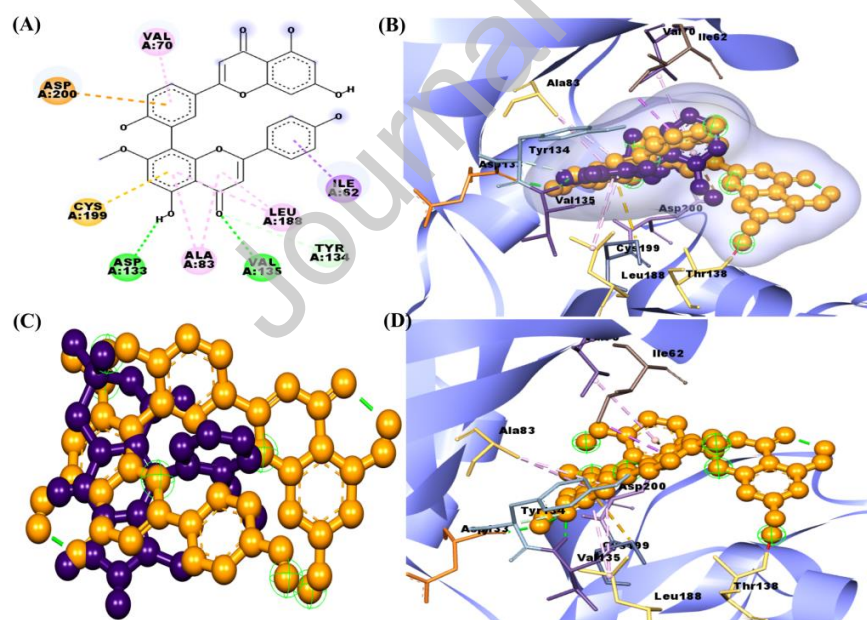


Fig. 8. (A) 2D interaction diagram showing the types of contacts formed between crystal structure of GSK3B receptor (PDB ID: 5HLP) and sotetsuflavone. The green dotted lines indicate H-bond. (B) Surface mapping of sotetsuflavone having golden color inside the active site of (PDB ID: 5HLP) along with reference molecule. The reference molecule is indicated in the purple color. (C) Represents the superimposed docked pose of

sotetsuflavone with reference molecule. **(D)** Represents the 3D interaction of sotetsuflavone at its active site. The protein structure is indicated in blue color; the ligand sotetsuflavone is indicated in golden color; the amino acid residues are indicated in the black color.

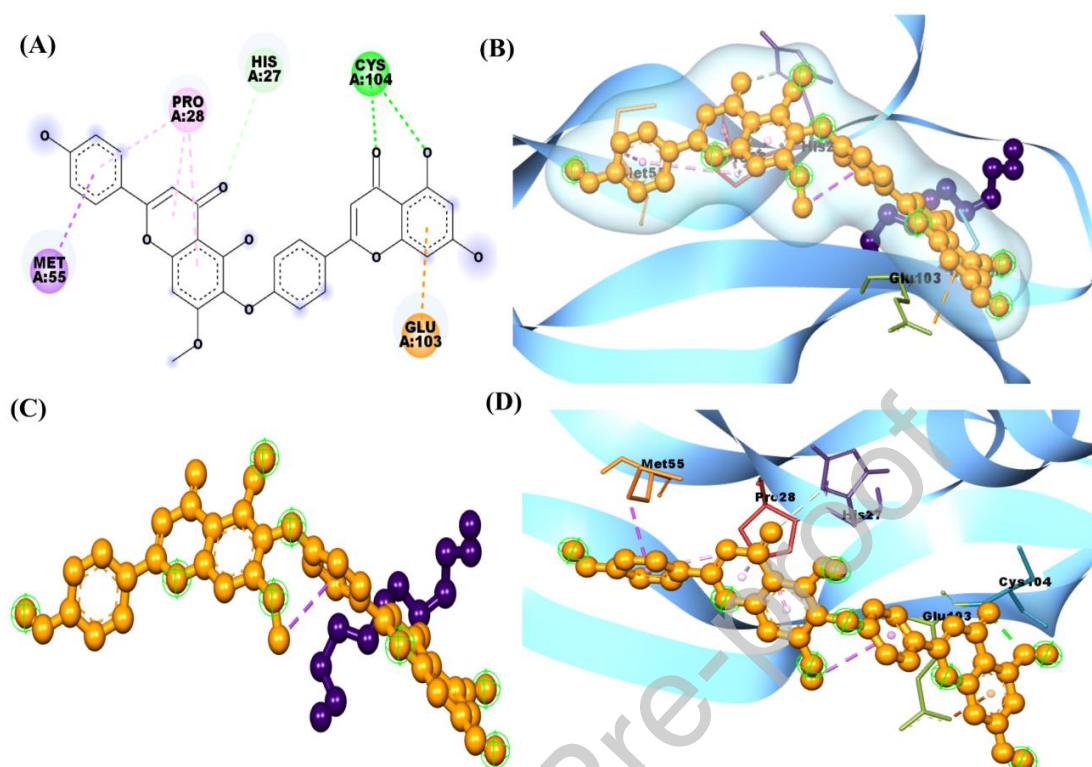


Fig. 9. **(A)** 2D interaction diagram showing the types of contacts formed between crystal structure of human VEGF-A receptor binding domain (PDB ID: 4KZN) and isocryptomerin. The green dotted lines indicate H-bonding. **(B)** Surface mapping of isocryptomerin having golden color inside the active site of (PDB ID: 4KZN) along with reference molecule. The reference molecule is indicated in the purple color. **(C)** Represents the superimposed docked pose of isocryptomerin with reference molecule. **(D)** Represents the 3D interaction of isocryptomerin at its active site. The protein structure is indicated in light blue color; the ligand isocryptomerin is indicated in golden color; the amino acid residues are indicated in the black color.

Isocryptomerin	-14.10	-13.90
Hinokiflavone	-9.90	-6.70
Sotetsuflavone	-9.80	-8.30
Isocryptomerin	-7.70	-3.50
	Phytochemical ΔG (kcal/mol)	Reference molecule ΔG (kcal/mol)

Fig. 10. Phytochemicals dock score comparison with the reference molecules for all the seven phytochemicals from the plant *Selaginella tamariscina*.

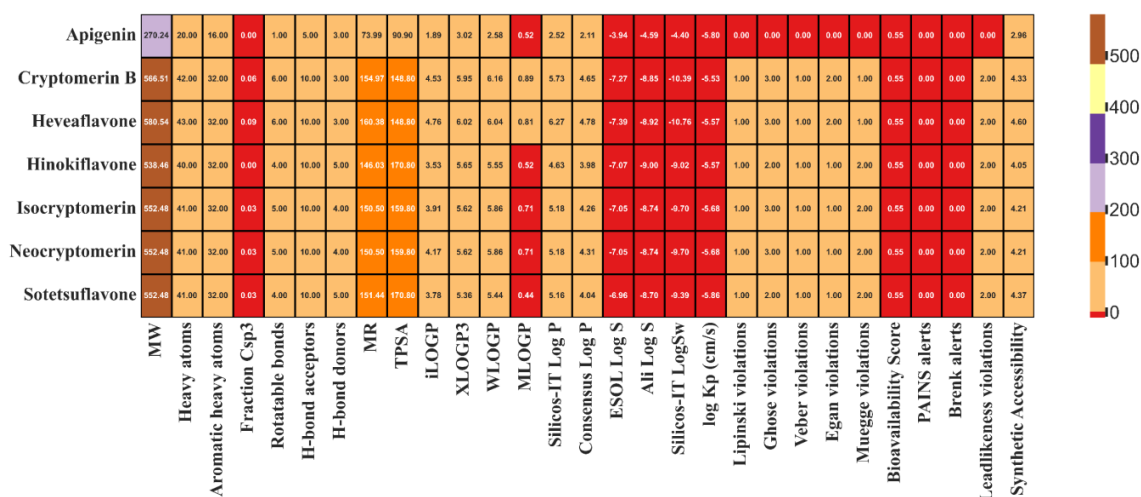


Fig. 11. ADME analysis for all the seven phytochemicals from the plant *Selaginella tamariscina*.

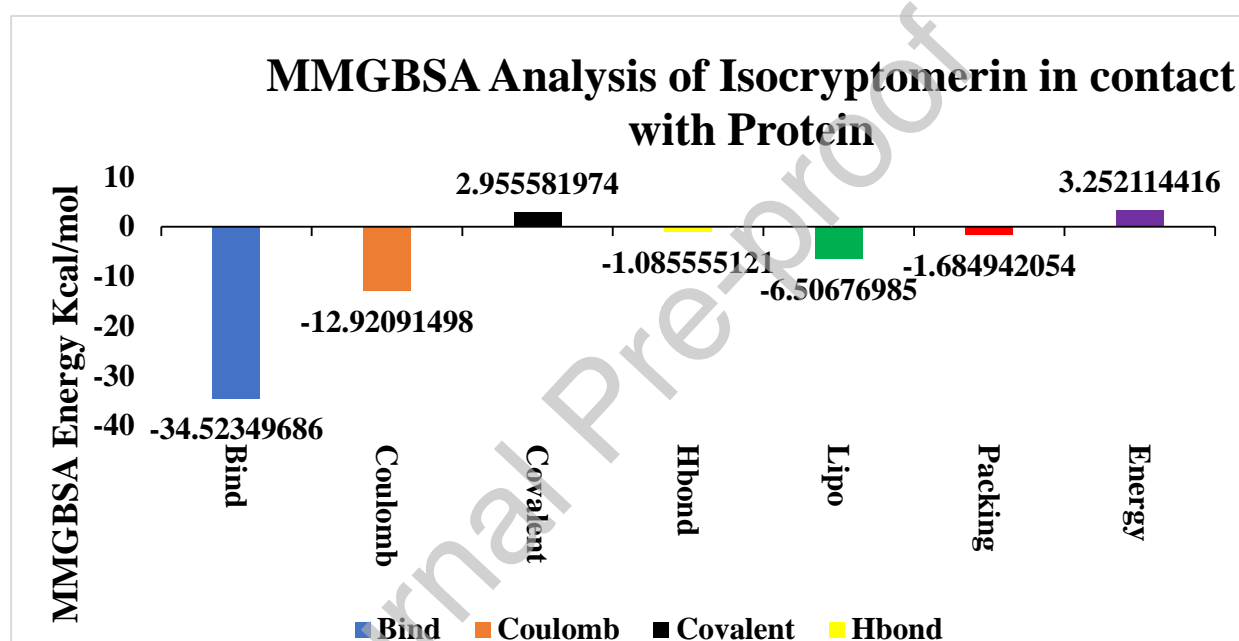


Fig. 12. MM-GBSA analysis of isocryptomerin and anticancer target AKT1 (PDB ID: 3O96) with different energies i.e. Binding free energy, Coulombic, Covalent, Hydrogen binding energy, Lipophilic, Generalized Born electrostatic solvation energy and Van der Waals binding energy.

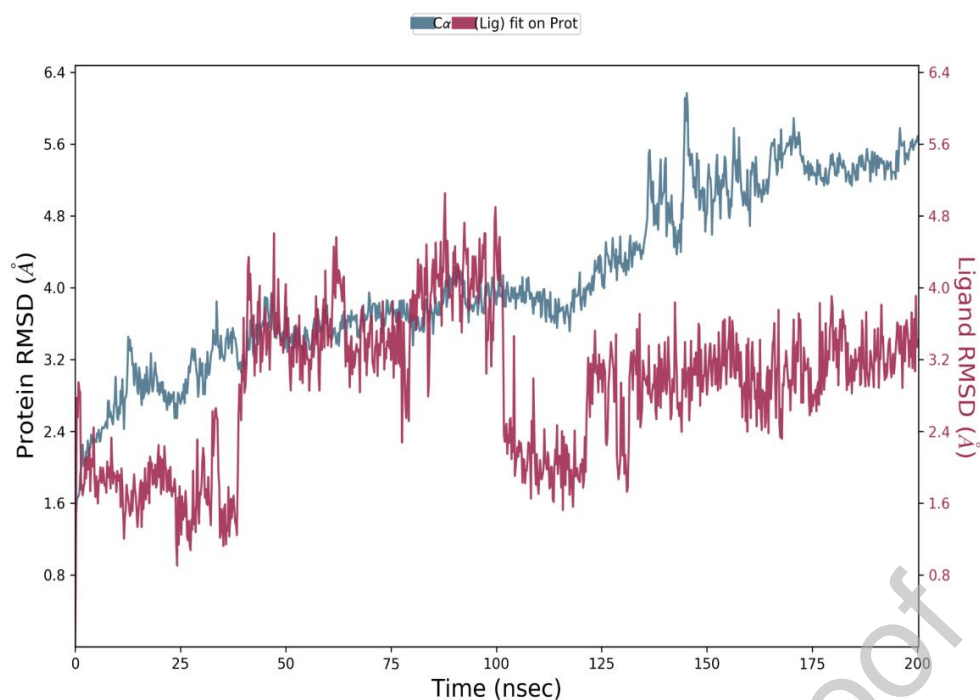


Fig. 13. RMSD analysis of the anticancer target AKT1 (PDB ID: 3O96) and phytochemical isocryptomerin with time. The left Y-axis show variation of protein RMSD while right Y-axis show ligand variation throughout the simulation.

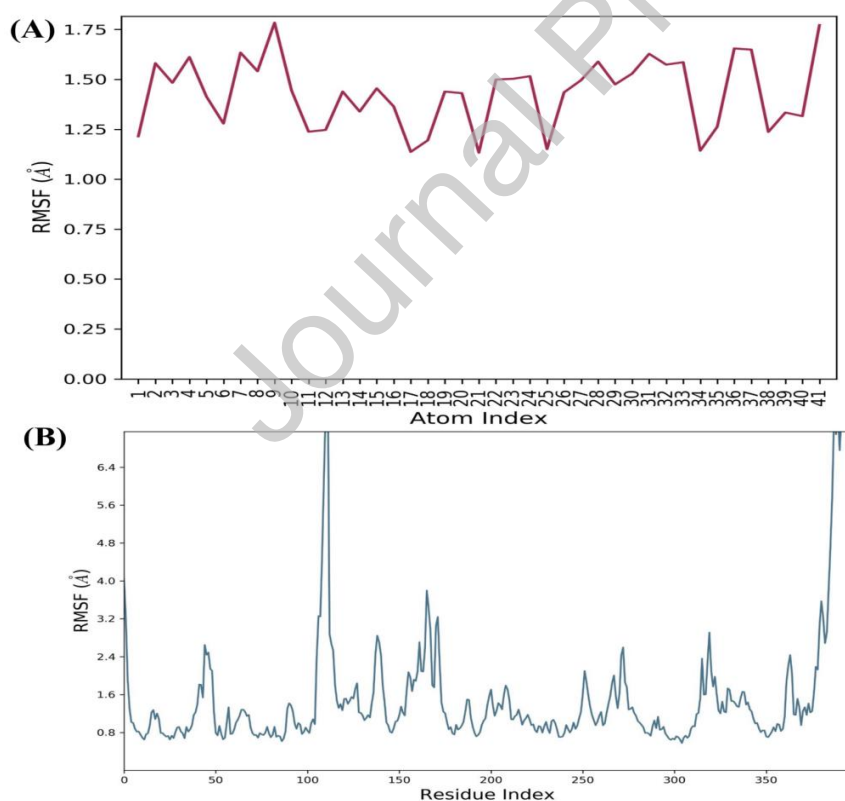


Fig.14. (A) and (B) show atom-wise RMSF of phytochemical isocryptomerin with respect to target protein AKT1 (PDB ID: 3O96) (lower panel) and ligand (upper panel).

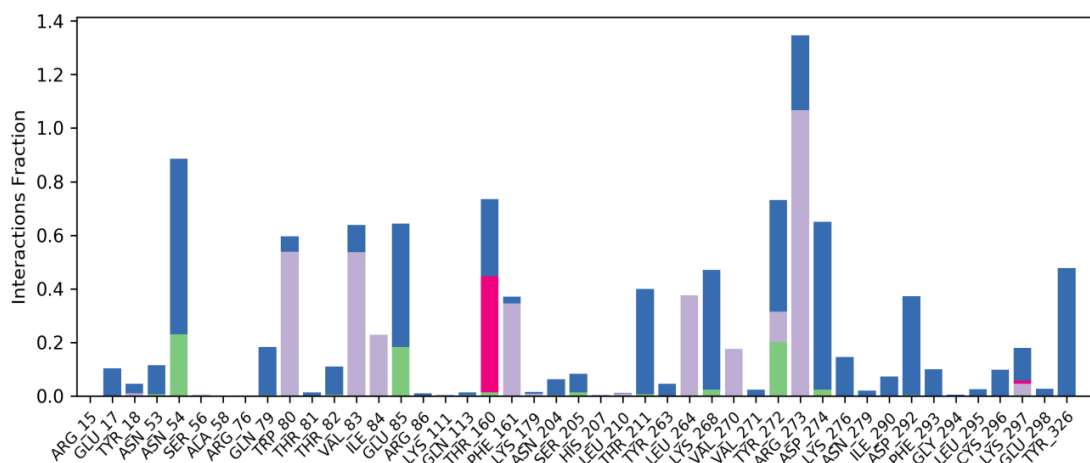


Fig. 15. Protein-ligand contacts histogram and ligand interaction (anticancer target AKT1 (PDB ID: 3O96) with phytochemical isocryptomerin).

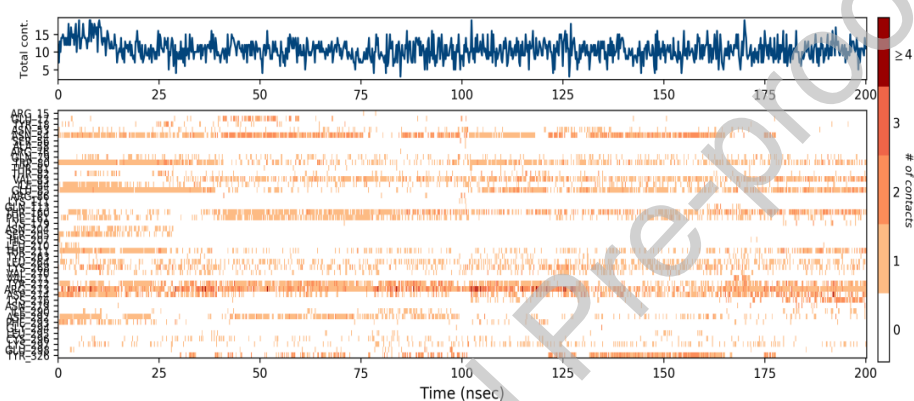


Fig. 16. A timeline representation of interactions and different contacts such as H-bonds, Ionic, Hydrophobic, and Water bridges (anticancer target AKT1 (PDB ID: 3O96) with phytochemical isocryptomerin).

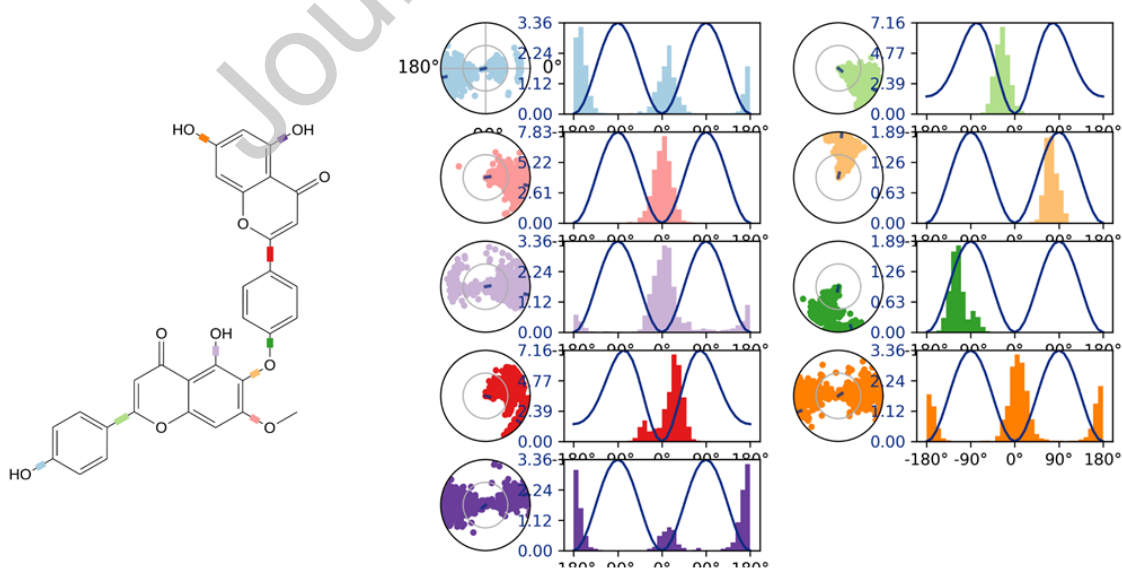


Fig. 17. The ligand torsions plot summarizes the conformational evolution of every rotatable bond (RB) in the ligand throughout the simulation trajectory (0.00 through 100.00 ns).

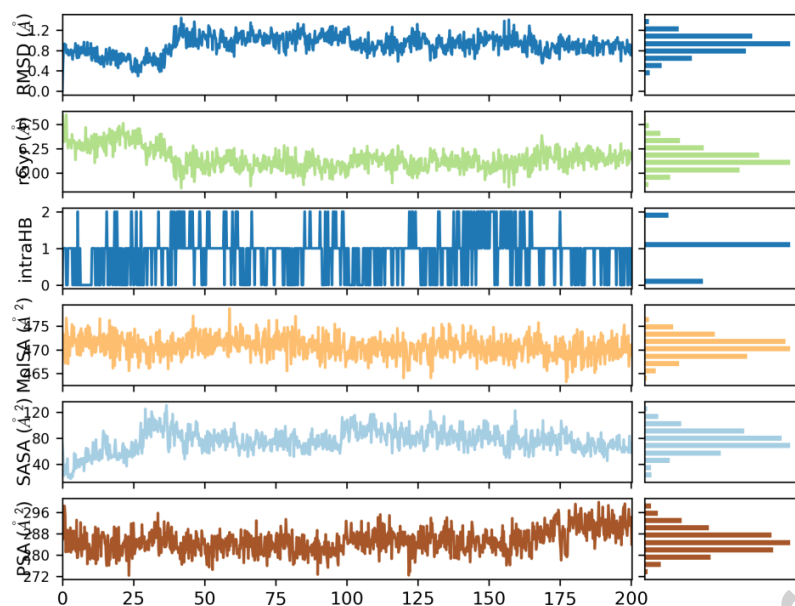


Fig. 18. Ligand properties Intramolecular Hydrogen Bonds (intraHB), Molecular Surface Area (MolSA), (Radius of Gyration (rGyr), Polar Surface Area (PSA) Solvent Accessible Surface Area (SASA) derived from MD simulations.

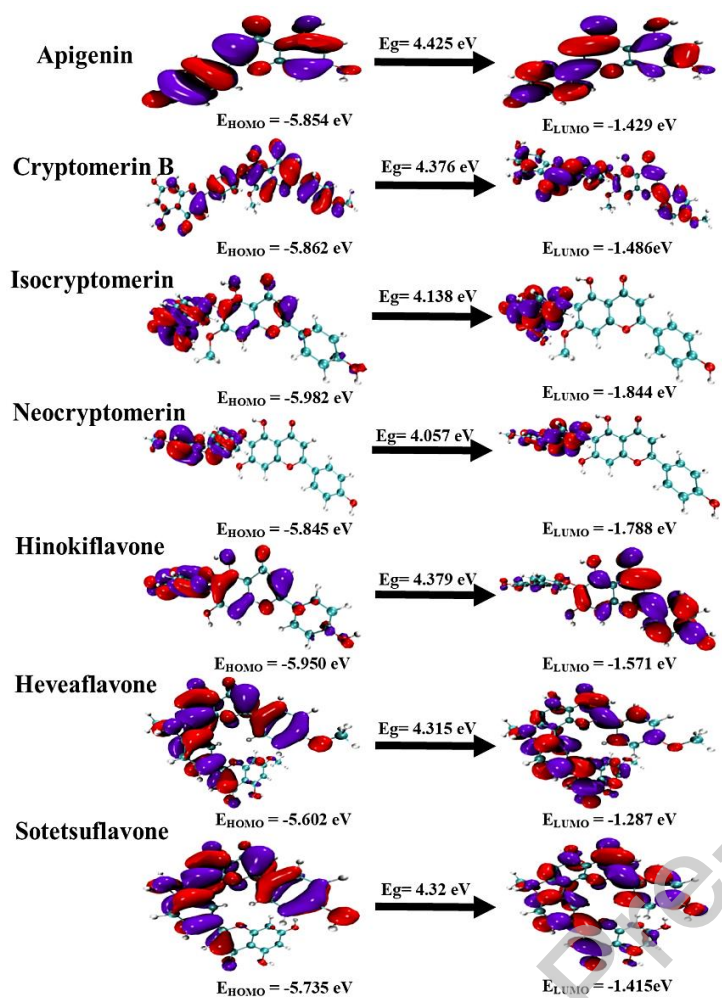


Fig. 19. Electron density regions shown by HOMO and LUMO analysis for all the seven phytochemicals from the plant *Selaginella tamariscina*.

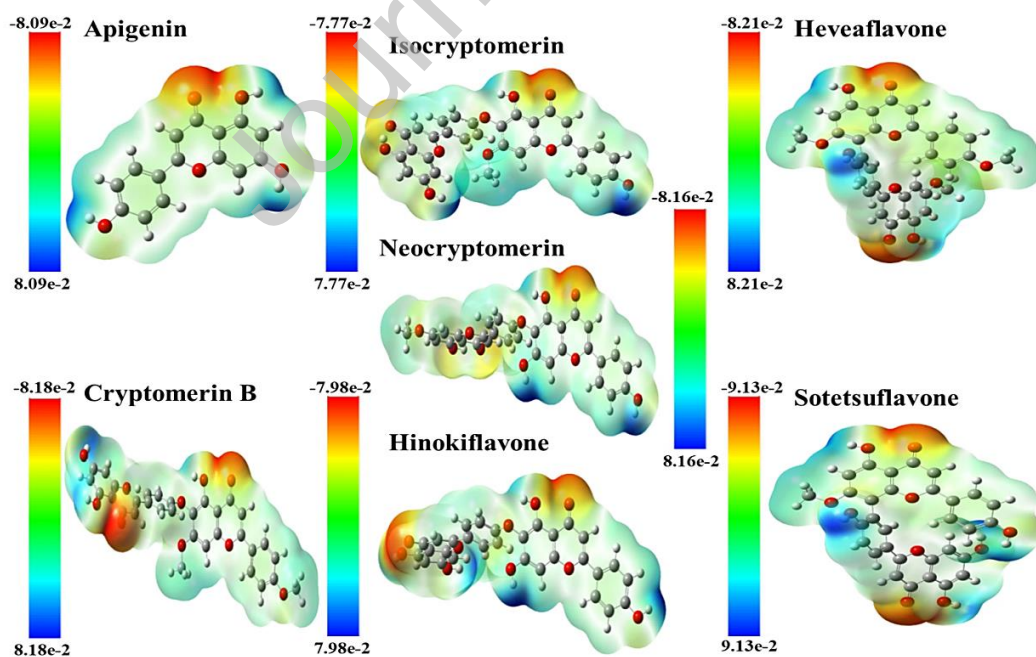


Fig. 20. Molecular electrostatic potential analysis for all the seven phytochemicals from the plant *Selaginella tamariscina*.

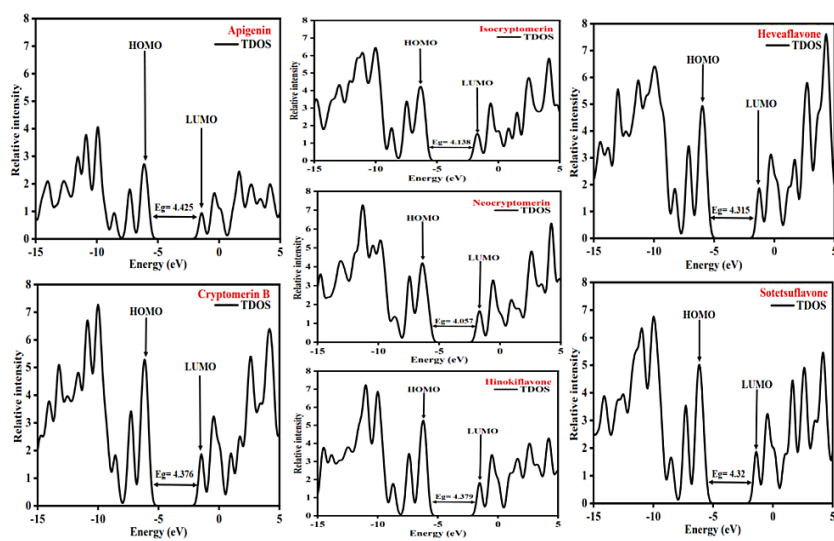


Fig. 21. Density of states analysis for all the seven phytochemicals from the plant *Selaginella tamariscina*.

Table 1. List of phytochemicals possessing anticancer activity against lung cancer along with their

	Phytochemicals	Phytochemical class	Biological source	Effective dose	Reference
<i>In-vivo</i> studies	Tanshinone	Quinones	Salvia miltiorrhiza	15 mg/kg	(Zhang et al., 2014)
	Emodin	Polyketides	Rheum palmatum	50 mg/kg	(He et al., 2012)
	4-Hydroxyderricin	Phenylpropanon	Angelica keiskei	50 mg/kg	(Sumiyoshi et al., 2015)
	Resveratrol	Phenolics	Grapes, mulberries, peanuts, and red wine	60 mg/kg	(Yousef et al., 2017)
	Honokiol	Phenolics	Magnolia species	10 mg/kg	(Singh et al., 2013)
	Shikonin	Naphthoquinones	Lithospermum erythrorhizon	2.0 mg/kg	(Lee et al., 2008)
	Chrysin	Flavonoid	Honey	250 mg/kg	(Mani and Natesan, 2018)
	Piperine	Alkaloid	Piper species	50 mg/kg	(Sriwiriyan et al., 2016)
	Homoharringtonine	Alkaloid	Cephalotaxus harringtonia	2.5 mg/kg	(Shi et al., 2020)
Clinical studies	Berberin	Alkaloid	Coptis chinensis	1000 ppm	(Paudel et al., 2022)
<i>In-vitro</i> studies	Acutiaporberine	Alkaloid	Thalictrum acutifolium	0.003 mol/ml	(Chen et al., 2002)
	Solamargine	Alkaloid	Solanum incanum	3 μ M	(Liang et al., 2004)
	Gigantol	Bibenzyls	Cymbidium goeringii	50 μ M	(Cho et al., 2016)
	β - D- digitoxose	Cardiac glycosides	Digitalis lanta	323 nM	(Kulkarni et al., 2016)
	Convallatoxin	Cardiac glycosides	Convallaria majalis	35 nM	(Schneider et al., 2016)
	Digitoxin	Cardiac glycosides	Digitalis purpurea	90.7 nM	(Elbaz et al., 2012)
	Apigenin	Flavonoid	Bell pepper	65.43 μ mol/l	(Zhou et al., 2017)
	Artocarpin	Flavonoid	Artocarpus species	10 μ M	(Tsai et al., 2017)

phytochemical class, effective dose and biological source.

Table 2. Bioactive compounds properties and their structure

Molecule Name	Molecular Weight	Drug Likeness (DL)	Oral Bioavailability (OB)	PubChem Id	Structure
Hinokiflavone	538.5g/mol	0.66	0.55	5281627	
Heveaflavone	580.5g/mol	0.59	0.55	15559724	
Neocryptomerin	552.5g/mol	0.68	0.55	5320065	
Isocryptomerin	552.5g/mol	0.75	0.55	5318537	
Apigenin	270.24g/mol	0.39	0.55	5280443	
Sotetsuflavone	552.5g/mol	0.43	0.55	5494868	
Cryptomerin B	566.5g/mol	0.6	0.55	5316145	

Table 3. Degree of seven phytochemical compounds explored through network analyzer cytoscape.

Phytochemical	Degree	Class
Apigenin	134	Flavonoids
Neocryptomerin	107	Flavonoids
Sotetusflavone	100	Bioflavonoids
Isocryptomerin	100	Flavonoids
Hinkoflavone	100	Bioflavonoids
Heavoflavone	100	Flavonoids
Cryptomerin B	100	Flavonoids

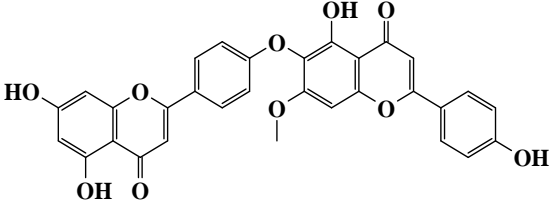
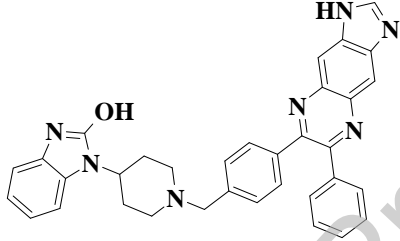
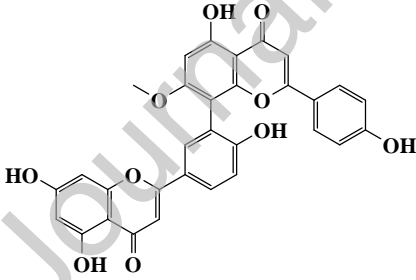
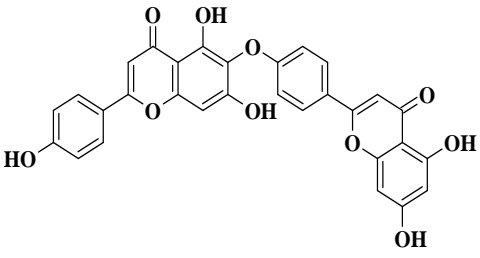
Table 4. Top seven genes ranked by degree method.

Gene Name	Degree score	Compounds	Pathways
AKT1	168	Apigenin	<ul style="list-style-type: none"> • Chemical carcinogenesis - reactive oxygen species • Pathways in cancer • PI3K-Akt signaling pathway • HIF-1 signaling pathway • Ras signaling pathway • EGFR tyrosine kinase inhibitor resistance • Lipid and atherosclerosis • Acute myeloid leukemia • PD-L1 expression and PD-1 checkpoint pathway in cancer • Kaposi sarcoma-associated herpesvirus infection • Endocrine resistance • AGE-RAGE signaling pathway in diabetic complications • Focal adhesion • Relaxin signaling pathway
VEGFA	156	Heavoflavone/ Apigenin	<ul style="list-style-type: none"> • Pathways in cancer • PI3K-Akt signaling pathway • HIF-1 signaling pathway • Ras signaling pathway • EGFR tyrosine kinase inhibitor resistance • Kaposi sarcoma-associated herpesvirus infection • AGE-RAGE signaling pathway in diabetic complications • Focal adhesion

			<ul style="list-style-type: none"> • Proteoglycans in cancer
			Relaxin signaling pathway
EGFR	134	cryptomerin B/ hinkoflavone/ neocryptomerin/ Apigenin	<ul style="list-style-type: none"> • Pathways in cancer • Chemical carcinogenesis - reactive oxygen species • PI3K-Akt signaling pathway • HIF-1 signaling pathway • Ras signaling pathway • Prostate cancer • EGFR tyrosine kinase inhibitor resistance • PD-L1 expression and PD-1 checkpoint pathway in cancer • Adherens junction • Endocrine resistance • Focal adhesion • Proteoglycans in cancer • Relaxin signaling pathway
GSK3B	64	hinkoflavone/ Heavoflavone neocryptomerin/apigenin/ cryptomerin B	<ul style="list-style-type: none"> • Pathways in cancer • Chemical carcinogenesis - reactive oxygen species • PI3K-Akt signaling pathway • HIF-1 signaling pathway • Ras signaling pathway • Arachidonic acid metabolism • Prostate cancer • EGFR tyrosine kinase inhibitor resistance • Lipid and atherosclerosis • Acute myeloid leukemia • PD-L1 expression and PD-1 checkpoint pathway in cancer • Adherens junction

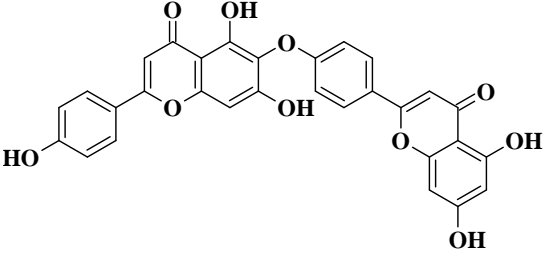
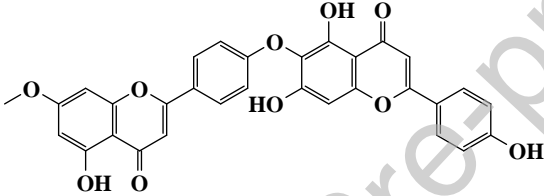
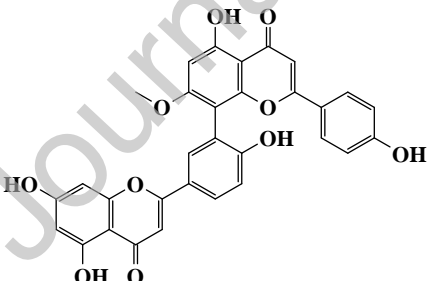
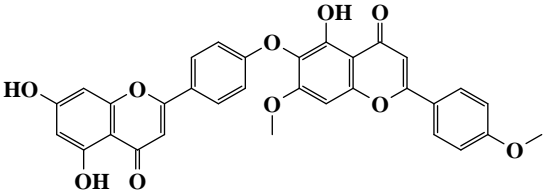
			<ul style="list-style-type: none"> • Kaposi sarcoma-associated herpesvirus infection • Endocrine resistance • Steroid hormone biosynthesis • AGE-RAGE signaling pathway in diabetic complications • Focal adhesion
PTGS2	112	Heavoflavone Neocryptomerin Apigenin/ hinkoflavone	<ul style="list-style-type: none"> • Pathways in cancer • Arachidonic acid metabolism • Kaposi sarcoma-associated herpesvirus infection
ESR1	126	cryptomerin B/ hinkoflavone/ Heavoflavone neocryptomerin/apigenin/ cryptomerin B	<ul style="list-style-type: none"> • Pathways in cancer • Endocrine resistance • Proteoglycans in cancer
SRC	124	neocryptomerin Apigenin/ cryptomerin B hinkoflavone Heavoflavone neocryptomerin	<ul style="list-style-type: none"> • Chemical carcinogenesis - reactive oxygen species • EGFR tyrosine kinase inhibitor resistance • Lipid and atherosclerosis • Adherens junction • Kaposi sarcoma-associated herpesvirus infection • Steroid hormone biosynthesis • Focal adhesion • Proteoglycans in cancer • Relaxin signaling pathway

Table 5. Molecular docking analysis of the phytochemicals with Crystal Structure of Human AKT1 PDB ID: 3O96 and comparison with reference molecule.

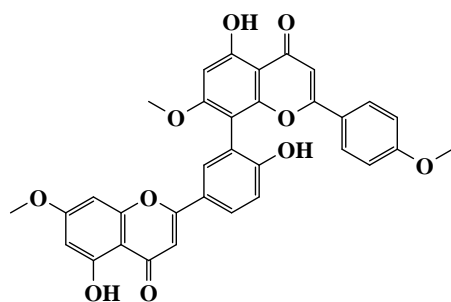
Phytochemical	Structure	Binding Energy ΔG (kcal/mol)	H-Bond interaction residues	Pi-Alkyl/Pi-Pi interacting residues
Isocryptomerin		-14.1	Tyr 272	Arg 273, Ile 84, Val 270, Gln 79, Trp 80, Lys 268, Cys 296
Reference ligand		-13.9	Arg 273	Val 270, Leu 264, Trp 80, Cys 296
Sotetsuflavone		-12.8	Val 271, Ala 58	Val 270, Trp 80, Lys 268, Leu 264, Tyr 272
Hinokiflavone		-12.2	Tyr 272	Asp 274, Arg 273, Ile 84, Thr 82, Gln 79, Val270, Trp 80, Lys 268, Cys 296

Neocryptomerin		-12.1	Ser 205	Asp 274, Thr 82, Arg 273, Ile 84, Leu 264, Val 270, Trp 80, Gln 79, Lys 268, Asp 292
CryptomerinB		-11.9	Val 271, Tyr 272	Arg 273, Ile 84, Trp 80, Val 270, Gln 79, Cys 296
Heveaflavone		-11.8	Gln 59	Trp 80, His 194 Ala 58, Leu 210, Leu 264, Lys 268, Val 270
Apigenin		-9.7	Gln 79, Asn 54, Ser 205, Ile 290, Thr 211	Val 270, Leu 264, Trp 80, Asp 292, Leu 210

Table 6. Molecular docking analysis of the phytochemicals with EGFR tyrosine kinase domain and reference molecule PDB ID: 1M17 and comparison with reference molecule.

Phytochemical	Structure	Binding Energy ΔG (kcal/mol)	H-Bond interaction residues	Pi-Alkyl/Pi-Pi interacting residues
Hinokiflavone		-9.9	Arg 817, Asn 818, Asp 831, Glu 734	Ala 719, Leu 820, Val 702, Phe 699
Neocryptomerin		-9.7	Arg 817, Asn 818	Leu 820, Leu 694, Val 702, Ala 719, Asp 831, Phe 699, Ile 735
Sotetsuflavone		-9.5	Thr 766, Asp 831	Cys 773, Phe 699, Leu 820, Val 702, Lys 721
CryptomerinB		-9.1	Leu 694, Met 769	Asp 776, Leu 820, Val 702, Ala 719

Heveaflavone

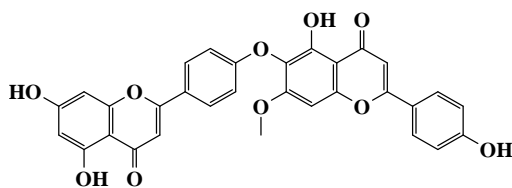


-9.1

Met 769

Val 702, Leu
694, Ala 719,
Lys 721, Met
742, Leu 764,
Leu 820

Isocryptomerin

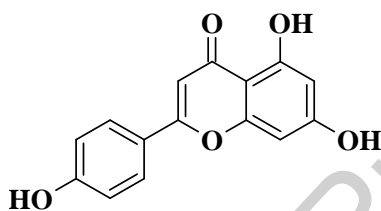


-9.1

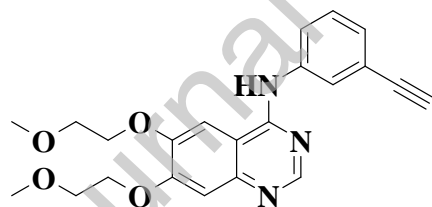
Met 769

Phe 771, Leu
694, Val 702,
Ala 719, Leu
820

Apigenin



-8

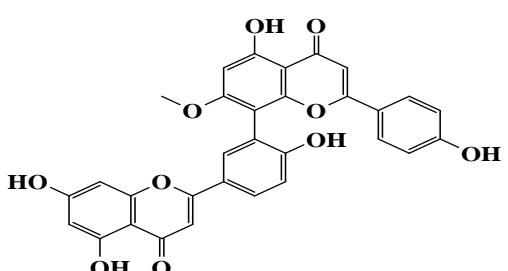
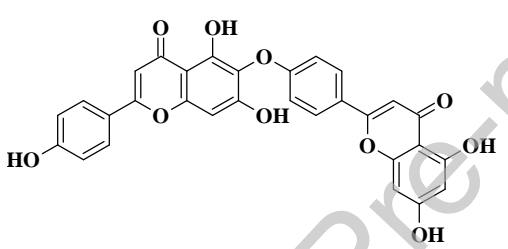
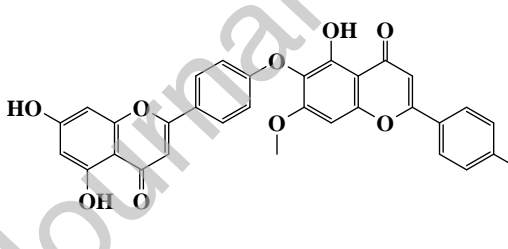
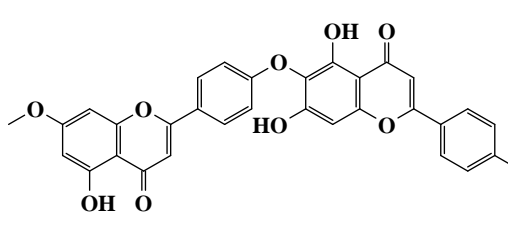
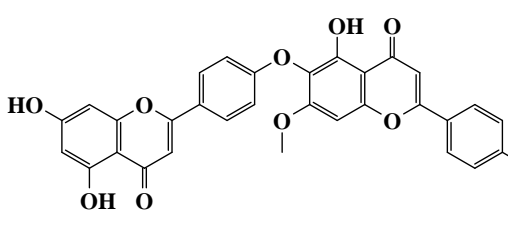
Leu 764, Leu 820, Leu
Thr 830, 694, Val 702,
Ala 719 Lys 721Reference
ligand

-6.7

Met 769

Val 702, Ala
719, Lys 721

Table 7. Molecular docking analysis of the phytochemicals with crystal structure of GSK3B with reference molecule PDB ID: 5HLP and comparison with reference molecule.

Phytochemical	Structure	Binding Energy ΔG (kcal/mol)	H-Bond interaction residues	Pi-Alkyl/Pi-Pi interacting residues
Sotetsuflavone		-9.8	Asp 133, Val 135	Asp 200, Cys 199, Ala 83, Leu 188, Ile 62, Val 70
Hinokiflavone		-9.5	Ser 219, Lys 85	Asp 181, Asp 200, Val 70, Ala 83, Cys 199, Leu 188
Isocryptomerin		-9.4	Arg 223, Val 135	Asp 181, Asp 200, Cys 199, Leu 188, Val 70, Ala 83
Neocryptomerin		-9.4	Cys 218, Ser 219, Asn 64, Lys 85	Leu 188, Ala 83, Val 70, Cys 199, Asp 200, Asp 181
CryptomerinB		-9	Asn 64, Lys 183, Tyr 220,	Ala 83, Leu Val 70, Phe 67, Lys

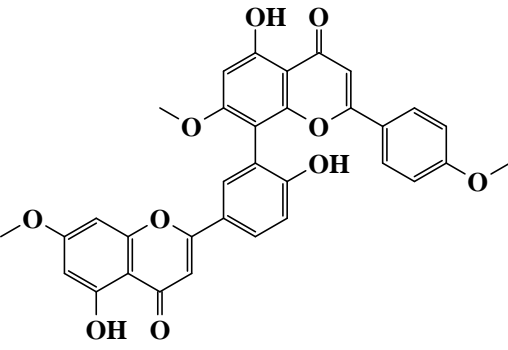
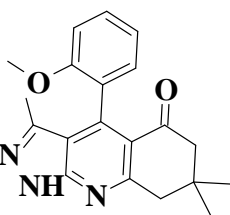
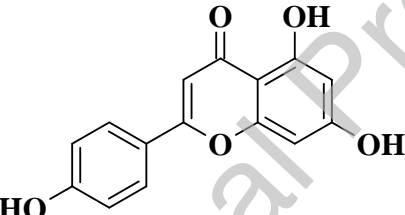
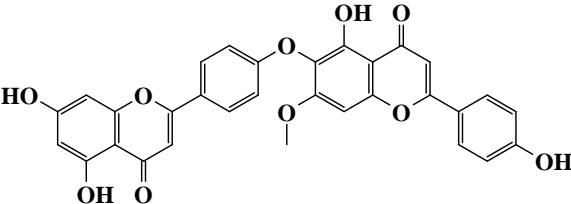
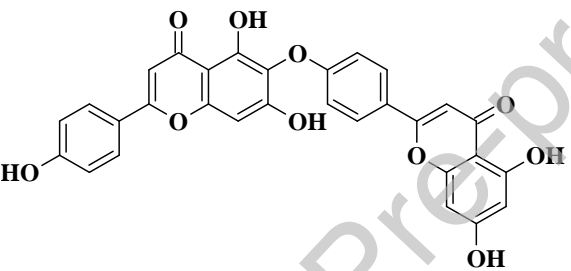
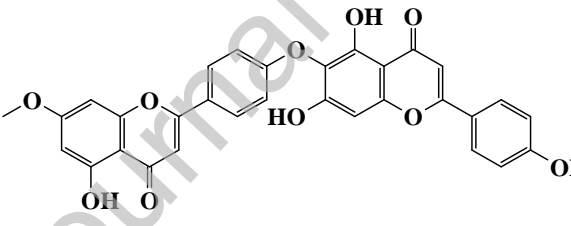
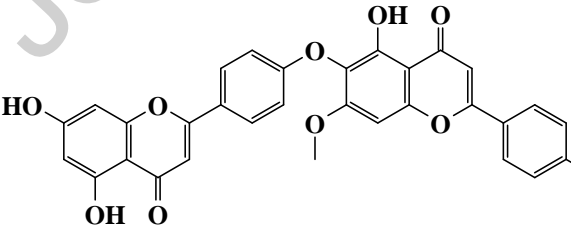
		222	85
Heveaflavone		-9	Lys 183, Asp 200, Val Asp 133, 70, Cys 199, Val 135 Arg 141, Ala 83, Leu 188, Ile 62, Leu 132
Reference ligand		-8.3	Val 135, Leu 188, Tyr Asp 133 134, Val 70, Ile 62, Cys 199, Ala 83
Apigenin		-7.4	Val 135, Tyr 134, Leu Asp 133 188, Ile 62, Val 70, Ala 83

Table 8. Molecular docking analysis of the phytochemicals with crystal structure of human VEGFA receptor PDB ID: 4KZN and comparison with reference molecule.

Phytochemical	Structure	Binding Energy ΔG (kcal/mol)	H-Bond interaction residues	Pi-Alkyl/Pi- Pi interacting residues
Isocryptomerin		-7.7	Cys 104	Met 55, Pro 28, Glu 103
Hinokiflavone		-7.6	Cys 104	Met 55, Pro 28, Glu 103
Neocryptomerin		-7.6	Cys 104	Met 55, Pro 28
CryptomerinB		-7.5	Cys 104, Gln 98	Met 55, Glu 103, Pro 28

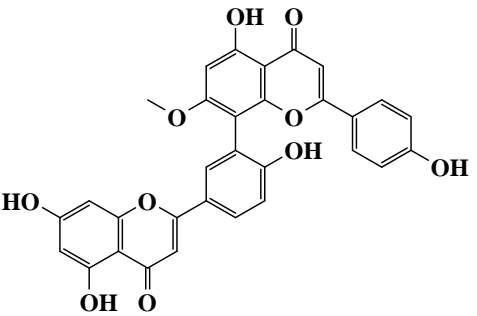
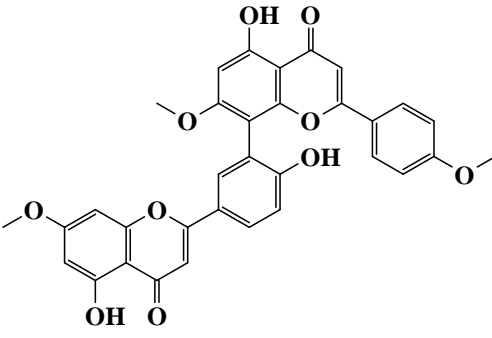
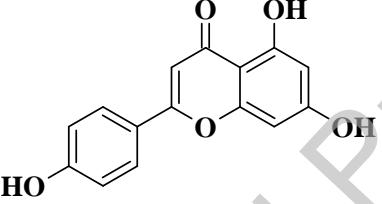
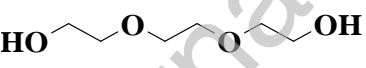
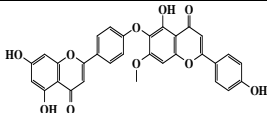
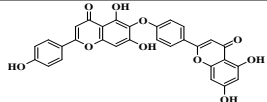
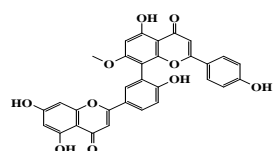
Sotetsuflavone		-7.2	Tyr 21, Tyr 25 Asn 62, Cys 61
Heveaflavone		-7	Gln 22, Tyr 25 Tyr 21, Asn 62
Apigenin		-5.8	Asn 62, Asp 63 Asp 63, Cys 61
Reference ligand		-3.5	Cys 68 -

Table 9. Molecular docking analysis of phytochemicals with four different crystallographic receptors and comparison with reference molecules.

Phytochemical	Receptor	Phytochemical ΔG (kcal/mol)	Reference molecule ΔG (kcal/mol)	H-Bond interaction residues	Vanderwaals interacting residues	Pi-Alkyl/Pi-Pi interacting residues
 Isocryptomerin	PDB ID: 3O96	-14.1	-13.9	Tyr 272	Val 83, Phe 161, Glu 85, Asp 274, Thr 82, Gly 294, Asp292, Leu 264, Ser 205, Asn 53, Val 271, Asn 54	Arg 273, Ile 84, Val 270, Gln 79, Trp 80, Lys 268, Cys 296
 Hinokiflavone	PDB ID: 1M17	-9.9	-6.7	Arg 817, Asn 818, Asp 831, Glu 734	Met 769, Gly 772, Leu 768, Thr 830,	Ala 719, Leu 694, Leu 820, Val 702, Phe 699

**Sotetsuflavone**

PDB ID: 5HL
P

-9.8 **-8.3** Asp 133, Val 135

Gly
695,
Leu
834,
Gly
833,
Ile
735,
Glu
738,
Lys
721

Phe 67, Asp 200, Cys 199, Ala 83,
Lys 85, Leu 188, Ile 62, Val 70

Phe
201,
Leu

132,
Val

110,
Tyr

134,
Arg

141,
Tyr

140,
Gln

185
Ile 76,

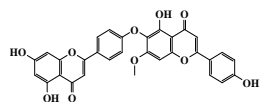
Gln 98,

His 99, Met 55, Pro 28, Glu 103

Asn

100,

Lys

**Isocryptomerin**

PDB ID: 4KZ
N

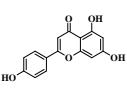
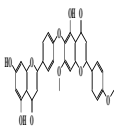
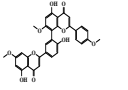
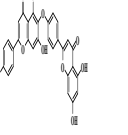
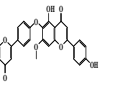
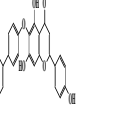
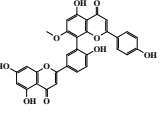
-7.7 **-3.5** Cys 104

101,
Tyr 25,
Cys
102,
Cys
26, His
27

Journal Pre-proof

Table 10. Chemical absorption, distribution, metabolism, and excretion (ADME) properties of the phytochemicals from the plant *selaginella tamariscina*.

Journal Pre-proof

Phytochemicals	Apigenin	Cryptomerin B	Hevealavone	Hinokilavone	Isocryptomerin	Neocryptomerin	Sotetsuflavone
Structure							
MW	270.24	566.51	580.54	538.46	552.48	552.48	552.48
Heavy atoms	20	42	43	40	41	41	41
Aromatic heavy atoms	16	32	32	32	32	32	32
Fraction Csp ³	0	0.06	0.09	0	0.03	0.03	0.03
Rotatable bonds	1	6	6	4	5	5	4
H-bond acceptors	5	10	10	10	10	10	10
H-bond donors	3	3	3	5	4	4	5
MR	73.99	154.97	160.38	146.03	150.5	150.5	151.44
TPSA	90.9	148.8	148.8	170.8	159.8	159.8	170.8
iLOGP	1.89	4.53	4.76	3.53	3.91	4.17	3.78
XLOGP3	3.02	5.95	6.02	5.65	5.62	5.62	5.36
WLOGP	2.58	6.16	6.04	5.55	5.86	5.86	5.44
MLOGP	0.52	0.89	0.81	0.52	0.71	0.71	0.44
Silicos-IT Log P	2.52	5.73	6.27	4.63	5.18	5.18	5.16
Consensus Log P	2.11	4.65	4.73	3.98	4.26	4.31	4.04
ESOL Log S	-3.94	-7.27	-7.39	-7.07	-7.05	-7.05	-6.96
ESOL Class	Soluble	Poorly soluble	Poorly soluble	Poorly soluble	Poorly soluble	Poorly soluble	Poorly soluble
Ali Log S	-4.59	-8.85	-8.92	-9	-8.74	-8.74	-8.7
Ali Class	Moderately soluble	Poorly soluble	Poorly soluble	Poorly soluble	Poorly soluble	Poorly soluble	Poorly soluble
Silicos-IT LogSw	-4.4	-10.39	-10.76	-9.02	-9.7	-9.7	-9.39
Silicos-IT class	Moderately soluble	Insoluble	Insoluble	Poorly soluble	Poorly soluble	Poorly soluble	Poorly soluble
GI absorption	High	Low	Low	Low	Low	Low	Low
BBB permeant	No	No	No	No	No	No	No
Pgp substrate	No	No	No	No	No	No	No
CYP1A2 inhibitor	Yes	No	No	No	No	No	No
CYP2C19 inhibitor	No	No	No	No	No	No	No
CYP2C9 inhibitor	No	Yes	No	Yes	Yes	Yes	Yes
CYP2D6 inhibitor	Yes	No	No	No	No	No	No
CYP3A4 inhibitor	Yes	No	No	No	No	No	No
log K _p (cm/s)	-5.8	-5.53	-5.57	-5.57	-5.68	-5.68	-5.86
Lipinski violations	0	1	1	1	1	1	1
Ghose	0	3	3	2	3	3	2

violations							
Veber							
violations	0	1	1	1	1	1	1
Egan							
violations	0	2	2	1	1	1	1
Muegge							
violations	0	1	1	2	2	2	2
Bioavailability							
Score	0.55	0.55	0.55	0.55	0.55	0.55	0.55
PAINS alerts	0	0	0	0	0	0	0
Brenk alerts	0	0	0	0	0	0	0
Leadlikeness							
violations	0	2	2	2	2	2	2
Synthetic							
Accessibility	2.96	4.33	4.6	4.05	4.21	4.21	4.37

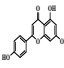
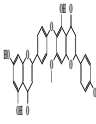
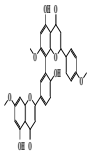
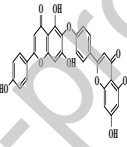
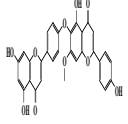
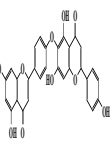
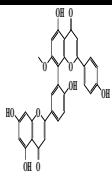
Phytochemicals	Apigenin	Cryptomerin B	Heveaflavone	Hinokiflavone	Isocryptomerin	Neocryptomerin	Sotetsuflavone
Toxicity Parameter							
hERG Blockers	---	-	---	---	---	---	---
H-HT	---	---	---	---	---	---	---
DILI	++	+++	+++	+++	+++	+++	+++
AMES Toxicity	-	-	-	-	-	-	-
Rat Oral Acute Toxicity	---	-	---	-	-	-	---
FDAMDD	-	+++	++	+++	+++	+++	++
Skin Sensitization	+++	+++	-	+++	+++	+++	++
Carcinogenicity	--	--	---	-	-	-	---
Eye Corrosion	---	---	---	---	---	---	---
Eye Irritation	+++	++	+	+++	++	++	++
Respiratory Toxicity	---	-	---	---	-	-	---
Mutagenic	Mild risk	No indication	No indication	No indication	No indication	No indication	No indication
Tumorigenic	No risk	Mild risk	No risk	No risk	No risk	No risk	No risk
Irritant	No	No	No	No	No	No	No
Reproductive effects	No effect	Mild risk	No effect	Mild risk	Mild risk	Mild risk	No effect

Table 11. Toxicity prediction of the phytochemicals from the plant *selaginella tamariscina*.

Table 12. Isocryptomerin properties determined via MD simulation i.e., Intramolecular Hydrogen Bonds (intraHB), RMSD, Molecular Surface Area (MolSA), Radius of Gyration (rGyr), Polar Surface Area (PSA), Solvent Accessible Surface Area (SASA).

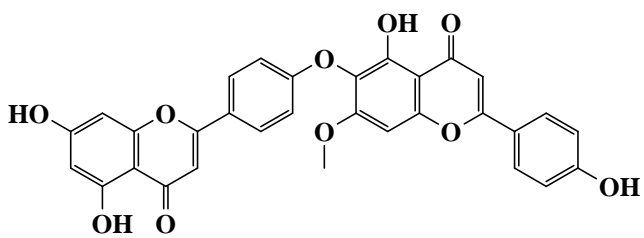
Ligand properties	RMSD	RGyr	intraHB	MolSA	SASA	PSA
 <p style="text-align: center;">Isocryptomerin</p>	1.2	30	2	76	120	295

Table 13. Calculated values of HOMO, LUMO, energy gap, hardness and softness analysis for all the seven phytochemicals from the plant *Selaginella tamariscina*.

Phytochemical	E_{HOMO}	E_{LUMO}	Eg	Hardness (η)	Softness (S)
Apigenin	-5.854	-1.429	4.425	2.212	0.452
Cryptomerin B	-5.862	-1.486	4.376	2.188	0.457
Isocryptomerin	-5.982	-1.844	4.138	2.069	0.483
Neocryptomerin	-5.845	-1.788	4.057	2.028	0.493
Hinokiflavone	-5.950	-1.571	4.379	2.189	0.456
Heveaflavone	-5.602	-1.287	4.315	2.157	0.463
Sotetsuflavone	-5.735	-1.415	4.32	2.160	0.462

Author Agreement Statement

We the undersigned declare that this manuscript is original, has not been published before and is not currently being considered for publication elsewhere.

We confirm that the manuscript has been read and approved by all named authors and that there are no other persons who satisfied the criteria for authorship but are not listed. We further confirm that the order of authors listed in the manuscript has been approved by all of us.

We understand that the Corresponding Author is the sole contact for the Editorial process. He/she is responsible for communicating with the other authors about progress, submissions of revisions and final approval of proofs

Signed by all authors as follows:

Date: 28/01/2023

Sunil Kumar

Sunil Kumar

Faheem Abbas

Faheem Abbas

Iqra Ali

Iqra Ali

Manoj K. Gupta

Manoj K. Gupta

Saroj Kumar

Saroj Kumar

Manoj Garg

Manoj Garg

Deepak Kumar

Deepak Kumar

Declaration of Competing Interest

The authors confirm that there are no known conflicts of interest associated with this publication and no significant financial support for this work that could have influenced its outcome.

Journal Pre-proof

[View publication stats](#)